Apical dominance control by TAR-YUC-mediated auxin biosynthesis is a deep homology of land plants

Mattias Thelander, Katarina Landberg, Arthur Muller, Gladys Cloarec, Nik Cunniffe, Stéphanie Huguet, Ludivine Soubigou-Taconnat, Véronique Brunaud, Yoan Coudert

Apical Dominance Control by *TAR-YUC*-Mediated Auxin Biosynthesis is a Deep Homology of Land Plants

Mattias Thelander[1], Katarina Landberg[1], Arthur Muller[2,3], Gladys Cloarec[2,4], Nik Cunniffe[5], Stéphanie Huguet[6,7], Ludivine Soubigou-Taconnat[6,7], Véronique Brunaud[6,7] and Yoan Coudert[2,*]

[1]Department of Plant Biology, Swedish University of Agricultural Sciences, The Linnean Centre for Plant Biology in Uppsala, SE-750 07, Uppsala, Sweden

[2]Laboratoire Reproduction et Développement des Plantes, Université de Lyon, ENS de Lyon, UCB Lyon 1, CNRS, INRA, INRIA, Lyon 69007, France

[3]Experimental Biology Research Group, Institute of Biology, Faculty of Sciences, University of Neuchâtel, 2000 Neuchâtel, Switzerland

[4]Institut Jean-Pierre Bourgin, INRAE, AgroParisTech, Université Paris-Saclay, 78000 Versailles, France

[5]Department of Plant Sciences, University of Cambridge, Downing Street, Cambridge CB2 3EA, UK

[6]Université Paris-Saclay, CNRS, INRAE, Univ Evry, Institute of Plant Sciences Paris-Saclay (IPS2), 91405 Orsay, France.

[7]Université de Paris, CNRS, INRAE, Institute of Plant Sciences Paris-Saclay (IPS2), 91405, Orsay, France

*Correspondence : yoan.coudert@ens-lyon.fr

Abstract

A key aim in biology is to identify which genetic changes contributed to the evolution of form through time. Apical dominance, the inhibitory effect exerted by shoot apices on the initiation or outgrowth of distant lateral buds, is a major regulatory mechanism of plant form[1]. Nearly a century of studies in the sporophyte of flowering plants have established the phytohormone auxin as a front-runner in the search for key factors controlling apical dominance[2,3], identifying critical roles for long-range polar auxin transport and local auxin biosynthesis in modulating shoot branching[4–10]. A capacity for lateral branching evolved by convergence in the gametophytic shoot of mosses and primed its diversification[11]; however, polar auxin transport is relatively unimportant in this developmental process[12], the contribution of auxin biosynthesis genes has not been assessed and, more generally, the extent of conservation in apical dominance regulation within the land plants remains largely unknown. To fill this knowledge gap, we sought to identify genetic determinants of apical dominance in the moss *Physcomitrium patens*. Here, we show that leafy shoot apex decapitation releases apical dominance through massive and rapid transcriptional reprogramming of auxin-responsive genes, and altering auxin biosynthesis gene activity. We pinpoint a subset of *P. patens TRYPTOPHAN AMINO-TRANSFERASE* (*TAR*) and *YUCCA FLAVIN MONOOXYGENASE-LIKE* (*YUC*) auxin biosynthesis genes expressed in the main and lateral shoot apices, and show that they are essential for coordinating branch initiation and outgrowth. Our results demonstrate that local auxin biosynthesis acts as a pivotal regulator of apical dominance in moss and constitutes a shared mechanism underpinning shoot architecture control in land plants.

Results and discussion

Massive and rapid reprogramming of auxin-responsive genes follows gametophore decapitation

Previous reports have shown that decapitation of the moss gametophore (*i.e.*, the gametophytic leafy shoot) tip promotes lateral branch formation, indicating conservation of apical dominance[12,13]. In the model species, *Physcomitrium patens*, gametophore branches arise *de novo* from epidermal cells in leaf axils, and initiation and outgrowth have been described as a single continuous development process[12]. To assess the dynamics of branch emergence following decapitation, we isolated *P. patens* gametophores from 4-week-old wild-type colonies, cut off their main apices and followed branch development over 48 hours. The first emerged branches were clearly visible 24 hours after decapitation (h.a.d.) and branches with well-developed leaves were observed 48 h.a.d., suggesting that the earliest molecular events leading to branching occur within a day (Figure 1A). To capture a comprehensive overview of the transcriptional changes associated with the release of apical dominance, we therefore analyzed the transcriptome of whole gametophores collected 2, 6, 12 and 24 h.a.d., and used gametophores collected immediately after decapitation (0 h.a.d.) as a reference. The proportion of genes whose transcription was affected increased up to 12 h.a.d., leading to a maximum of 5028 and 4734 genes down- and up-regulated, respectively, suggesting that major transcriptional changes occur before the first branches become visible (Tables S1 and S2, Figure S1 and S2). In an attempt to specifically address the contribution of auxin-related genes in apical dominance, we then compared the effect of auxin and decapitation at the transcriptional level. We sequenced the transcriptome of 4-week-old wild-type gametophores treated with indole-3-acetic-acid (IAA) for 30 minutes and used mock-treated plants as a reference to identify early auxin-responsive genes. We found that 3652 and 4524 genes were down- and up-regulated by IAA, respectively (Tables S1 and S3). By cross-referencing decapitation and IAA-regulated gene sets, we observed a striking global anti-correlation between both treatments (Figure 1B). Sixty-four percent of genes down-regulated 2 h.a.d. were IAA-induced, whilst only 5% were IAA-repressed. A similar trend was observed for “6 h.a.d.” and “12 h.a.d.” gene sets. For example, both *ARF* and *AUX/IAA* auxin signalling genes, previously identified as early auxin-responsive genes[14], responded oppositely in that most genes were induced by IAA and repressed after decapitation (Figure 1C). Inversely, 46% of genes up-regulated 2 h.a.d. were IAA-repressed, whilst only 14% were IAA-induced, with a similar trend for “6 h.a.d.” and “12 h.a.d.” gene sets (Figure 1B). Chi-squared tests revealed a significant association between IAA repression/induction and decapitation repression/induction at all four times, and the response was stronger at early

time points ($\chi_1^2 = 1915, p < 0.001$ at 2 h.a.d; $\chi_1^2 = 2731, p < 0.001$ at 6 h.a.d.; $\chi_1^2 = 2007, p < 0.001$ at 12 h.a.d.; $\chi_1^2 = 6.855, p = 0.009$ at 24 h.a.d.). Thus, the largely antagonistic transcriptional responses of decapitated and auxin-treated gametophores suggest a major contribution of auxin and its targets in apical dominance control in moss. Moreover, these data support the notion that the main gametophore apex is an auxin source with long-range effects[12,15].

Decapitation rapidly alters *TAR* and *YUC* auxin biosynthesis gene expression

Auxin is mainly produced from a tryptophan (TRP)-dependent biosynthetic pathway in land plants[16]. TRP is converted to indole-3-pyruvic acid (IPyA) by TRYPTOPHAN AMINO-TRANSFERASE (TAA/TAR) enzymes, that is then converted to auxin by YUCCA FLAVIN MONOOXYGENASE-LIKE (YUC) enzymes[17]. Previously published works in the flowering plant *Arabidopsis thaliana* have proposed that auxin depletion from the leaf axil is needed to promote axillary meristem formation[9,10]. In contrast, the subsequent inhibition of axillary bud outgrowth depends on expression of *AtTAA1/WEI8*, *AtTAR2*, *AtYUC1*, *AtYUC4* and *AtYUC6* auxin biosynthesis genes in partially overlapping domains of the shoot apical meristem[6,7]. Double and triple mutants in these genes, including *yuc1yuc4*, *yuc1yuc4yuc6* and *taa1tar2* allele combinations, show various degrees of decreased apical dominance reflected by an enhanced development of branches. We reasoned that our dataset would provide a reference to test the extent to which the role of auxin biosynthesis genes in apical dominance control is shared between *A. thaliana* and *P. patens*. Auxin metabolite profiling in various genetic backgrounds has shown that both steps of TRP-to-IAA conversion occur in *P. patens*[15,16]. To determine the changes in auxin biosynthesis gene activity during the release of apical dominance, we therefore retrieved *PpTAR* (named *TAR* hereafter for the sake of readability) and *PpYUC* (named *YUC* hereafter) expression profiles from our RNA-seq data. We identified two *TAR* and three *YUC* genes that were significantly differentially expressed after decapitation (Figure 1D and 1E). Specifically, *TARA*, *TARC* and *YUCF* were induced as early as 2 h.a.d., *YUCC* was induced from 12 h.a.d., and *YUCB* was repressed. We also found that the expression of *TARA*, *YUCE* and *YUCF*, but not *TARC*, *YUCB* and *YUCC*, was affected by exogenous auxin, suggesting that auxin may to some extent regulate its own biosynthesis. Thus, our data suggest that decapitation alters auxin biosynthesis elsewhere in the gametophore.

***TAR* and *YUC* genes are mainly active in the apical and basal portions of gametophores**

To determine the overall expression patterns of *TARA, TARC, YUCB, YUCC* and *YUCF* genes, we analysed the activity of transcriptional fusions between corresponding promoter regions and a GFP-GUS chimeric protein transformed in a wild-type background (Figure S3). We found that the spatial expression domains of *TAR* and *YUC* promoters largely overlapped in whole gametophores. Beta-glucuronidase (GUS) activity was detected at the main apex, at the base, notably in rhizoid cells, and in discrete regions of the stem corresponding to initiating branch apices (Figure 2A, 2D, 2G, 2J and 2M). At the main apex, *TAR* promoters are active in the apical cell and emerging leaves[15], and both *TAR* and *YUC* promoter activity were also observed in axillary hair cells surrounding the gametophore apical cell, reminiscent of the expression pattern of auxin-related genes like *PpSHI1* and *PpSHI2*[18] (Figure 2P and 2Q). Expression of *TAR* and *YUC* genes in isolated gametophore apices was confirmed by quantitative RT-PCR (Figure S4). Promoter activity of *YUCF*, and to a lesser extent *YUCB* and *YUCC*, was also detected in axillary hair cells elsewhere on the stem (Figure 2M, 2R). This indicates that the expression of *TARA* and *TARC* is more restricted in space than that of *YUCB*, *YUCC* and *YUCF*, and it is unlikely that auxin biosynthesis occurs in leaf axils in the absence of *TAR* activity.

Activation of *TAR* and *YUC* gene expression accompanies branch formation

To determine how decapitation affected the activity of selected transcriptional reporters, gametophores were collected 24 hours after apex excision and stained for GUS activity, thereby leaving enough time for new branches to initiate and grow out. The intensity of GUS accumulation patterns remained overall similar to intact controls, except for the *YUCB* promoter that seemed more weakly expressed after decapitation, likely reflecting its transcriptional repression (Figure 1E). The spatial distribution of these patterns was changed in leaf axils where we observed an activation of *TARA, TARC, YUCB, YUCC* and *YUCF* promoter expression associated with the formation of new branches. The activity of *TARA* and *TARC* promoters was detected from the earliest stage of branch formation, throughout the branch initium (Figures 2B, 2C, 2E and 2F). In contrast, *YUCB*, *YUCC* and *YUCF* promoter activity were first detected at a later stage when the first leaves were clearly visible, and mostly in hair cells of the branch apical region (Figures 2H, 2K, 2N). At a more mature stage of branch development, *i.e.* when leaves and brown rhizoids were well-developed, *TAR* and *YUC* promoters were active in overlapping spatial domains mirroring those described previously in whole gametophores (Figures 2I, 2L and 2O, data not shown for *TARs*). Expression of *TAR* and *YUC* genes in newly emerged branches taken from decapitated gametophores was further validated by quantitative RT-PCR (Figure S4). The temporal delay

between *TAR* and *YUC* promoter activation and the differences in their spatial expression domains at early stages of branch initiation suggest that IPyA might be transported from the meristematic cells where it is synthesized to adjacent hair cells to be converted to auxin by YUC enzymes. Alternatively, these differences might be explained by the short-range movement of *TAR* or *YUC* mRNA, or corresponding proteins; the involvement of *YUC* genes expressed in the gametophore but not detected in our differential gene expression analysis, such as *YUCE* (Figure S5); or unmask a putative YUC-independent function of IPyA. Together, the above data suggest that TRP-dependent auxin biosynthesis occurs primarily in the main apex and the basal portion of gametophores, and resumes locally in initiating branches during development.

TAR and _YUC_ genes have dual roles in branch initiation and outgrowth

To investigate the function of decapitation-induced *TAR* and *YUC* genes in gametophore branching, we grew corresponding single and double knock-out mutants for 5-8 weeks and quantified their branching patterns, as done previously[12] (Figure 3, Figure S6). We found that *tara* and *tarc* single mutants had overall similar phenotypes to control plants (Figure S7), and observed only minor perturbations of the branch distribution patterns in *yucc* and *yucf* single mutants (Figure S8). In contrast, both *tarac* and *yuccf* double mutants had a shorter apical inhibition zone and inter-branch distance, and an increased branch density with respect to corresponding controls, suggesting that apical dominance and lateral inhibition from branch tips were significantly weaker in auxin biosynthesis mutants (Figure 3A-3H, 3K-3L and 3M-3N). These data provide the first direct evidence that auxin biosynthesis genes active in gametophore apices coordinate branch patterning at a distance, thus demonstrating the central hypothesis of a previously published model of branching control[12]. We also observed that the position of the lowermost branch was closer to the gametophore base in *tarac* and *yuccf* mutants than in corresponding wild-type controls (Figure 3O). Moreover, the number of branches in the three most basal metamers was much higher in *tarac* (n = 23 branches) and *yuccf* gametophores (n = 15) than in wild-type controls (n = 5 and 3, respectively), suggesting that local auxin biosynthesis prevents branching at the gametophore base (Figures 3A-3D). A CAROTENOID CLEAVAGE DIOXYGENASE 8 (CCD8)-derived cue belonging to the strigolactone family of compounds has previously been proposed to suppress branching at the gametophore base[12,19], and *in vitro* characterization of PpCCD8 enzymatic activity indicates that this molecule may be the strigolactone precursor carlactone[20]. These data suggest that auxin could act concomitantly with carlactone to fulfil this inhibitory role, and their mode of interaction remains to be seen. Despite the overall

increase in branch number in *tarac* mutants, we observed strong disparities in the branch distribution pattern between gametophores. Whilst some gametophores bore branches on up to six consecutive metamers, others had few or no visible branches at all, which was rather counter-intuitive (Figure 3B). However, on closer inspection of *tarac* gametophores, we noticed that tiny arrested branches were nested in most leaf axils lacking a visible branch (Figure 3I-3J), reminiscent of dormant buds observed in other plants. We found that branch formation was suppressed by exogenous auxin application in *tarac* mutants, as well as *TARA* overexpression (Figure S9). This suggests that in normal conditions, low *TAR* activity triggers branch formation, whilst relatively higher *TAR* activity is necessary to promote branch development at later stages. Thus, branch initiation and outgrowth are separable processes that are coupled during development through controlled spatio-temporal changes in auxin levels, similar to the mechanism coordinating axillary meristem formation and outgrowth in flowering plants[21].

This work aimed to research genetic determinants involved in the regulation of apical dominance in the gametophytic shoot of a moss. We have taken a comparative transcriptome approach, showing that early auxin-responsive genes dominate in the response of gametophores to decapitation, and identified *TAR* and *YUC* auxin biosynthesis genes acting redundantly in the main gametophore apex and branch apices. Perturbations of branching patterns measured in *tarac* and *yuccf* mutants are consistent with a role of corresponding genes in apical dominance control. In the future, our dataset should enable to explore further the mode of auxin action and, notably, the interplay with putative shared regulators of apical dominance revealed in gene ontology enrichment analyses, such as trehalose-6-phosphate metabolic enzymes[22–25] and APETALA2/ETHYLENE RESPONSIVE ELEMENT BINDING PROTEIN transcription factors[26–29] (Tables S2 and S3, Figures S10 and S11). Our dataset also contains genes of uncharacterized function whose transcription was not affected by auxin, representing an untapped reservoir of putative regulators of shoot architecture.

From an evolutionary perspective, the *TAR-YUC*-dependent auxin biosynthesis pathway originated in streptophyte algae and is conserved in all extant land plant lineages[30,31]. For instance, the genome of the liverwort *Marchantia polymorpha* contains one functional *MpTAA* gene and two *MpYUC* genes, named *MpYUC1* and *MpYUC2*[32]. Similar to our observations in the moss gametophore, *MpYUC2* expression domain is broader than that of *MpTAA* in the liverwort thallus (*i.e.,* the leafless gametophytic body), and both domains overlap in meristematic notches that contain the apical stem cells at the origin of thallus tissues. Whilst thallus branching occurs by apical notch dichotomy that is developmentally distinct from

lateral branching in the moss gametophore[33,34], *M. polymorpha taa* and *yuc* knock-down plants also display hyperbranching phenotypes. Together with data previously collected in *A. thaliana* and our novel findings in *P. patens*, this suggests that a conserved molecular mechanism driving auxin biosynthesis operates locally, in morphologically distinct meristematic structures, and coordinates various branching modes in bryophytes and vascular plants. Although this is still disputed, the most recent molecular phylogenies have resolved bryophytes (including *P. patens* and *M. polymorpha*) as a monophyletic lineage, sister to the vascular plants (including *A. thaliana*), and both lineages could have diverged from their last common ancestor in the Cambrian period (541-485 My ago)[35–37]. The exact nature and morphology of this ancestor remains largely inaccessible, but combined evidence from phylogeny and the fossil record points towards a leafless body with dichotomously branched gametophytic axes bearing nutritionally-dependent and unbranched sporophytes[38–40]. Lateral branching, where branches form on the side of growing axes in association with leaves or phyllids (*i.e.*, the leaf-like organs of bryophytes), is therefore a derived trait which arose by convergence in moss gametophytes and vascular plant sporophytes[33]. In contrast with the classical definition of homology which implies a historical continuity in the evolution of morphological traits, the notion of deep homology that defines 'the sharing of the genetic regulatory apparatus used to build morphologically and phylogenetically disparate features' applies here[41,42]. We conclude that the involvement of *TAR-YUC*-mediated auxin biosynthesis to regulate apical dominance and shoot branching represents a remarkable case of deep homology in land plants.

Material and methods

Physcomitrium patens plant growth and transformation

The Gransden strain of *Physcomitrium patens* was used for RNA-seq experiments, and the Reute[43] strain that is more fertile in laboratory conditions was used as the wild-type (WT) background for generating all the transgenic lines. Moss colonies were initiated from 1 mm^2 spot cultures and cultivated for 4-5 weeks (unless otherwise stated) in sterile Magenta GA-7 tissue culture vessels (Bioworld, Dublin, OH, USA) on BCDAT medium (250 mg/L $MgSO_4.7H_2O$, 250 mg/L KH_2PO_4 (pH 6.5), 1010 mg/L KNO_3, 12.5 mg/L, $FeSO_4.7H_2O$, 0.001% Trace Element Solution (0.614 mg/L H_3BO_3, 0.055 mg/L $AlK(SO_4)_2.12H_2O$, 0.055 mg/L $CuSO_4.5H_2O$, 0.028 mg/L KBr, 0.028 mg/L LiCl, 0.389 mg/L $MnCl_2.4H_2O$, 0.055 mg/L $CoCl_2.6H_2O$, 0.055 mg/L $ZnSO_4.7H_2O$, 0.028 mg/L KI and 0.028 mg/L $SnCl_2.2H_2O$), 0.92 g/L di-ammonium tartrate ($C_4H_{12}N_2O_6$) and 8 g/L agar with $CaCl_2$ added to a 1 mM concentration after autoclaving, at 23°C under a 16h light/8h dark cycle, at 50-150 $\mu mol.m^{-2}.s^{-1}$ in MLR-352 growth cabinets (PHCbi, Etten-Leur, The Netherlands). Genetic transformation was performed as described in Coudert *et al*. (2019)[44].

Decapitation and auxin treatments

For pharmacological treatments of wild-type gametophores, a 70% ethanol solution containing 100 mM indole-3-acetic acid (IAA) (Merck KGaA, Darmstadt, Germany) was diluted 10,000 times in water to reach a final concentration of 10 μM IAA. A 70% ethanol solution was diluted 10,000 times in water and used as a mock control. Moss cultures were soaked in diluted solutions for 30 minutes before tissue harvest. For decapitation, gametophores were teased apart from moss colonies with thin tip tweezers, planted in an upright position on BCDAT petri dishes and their apical portion was cut off with micro-scissors, as described in Coudert, Palubicki *et al.* (2015)[12]. For pharmacological treatments of *tarac* mutants, a 95% ethanol solution containing 1 mM indole-3-acetic acid (IAA) (Duchefa Farma B.V., Haarlem, Netherlands) was diluted 1,000 times in water to reach a final concentration of 1 μM IAA. A 95% ethanol solution was diluted 1,000 times in water and used as a mock control. Moss cultures were soaked in diluted solutions for 24 hours 3, 5 and 7 weeks after protonema inoculation.

Generation of *YUC* transcriptional reporters and *yuc* mutants

All the transgenic lines used in this study are listed in Table S4. Generation and confirmation of the transcriptional reporter lines *TARA::GFP-GUS*, *TARC::GFP-GUS*, and *YUCF::GFP-GUS*, as well as the knockout lines *tara*, *tarc*, *tarac*, *yucc*, and *yucf* have been previously

described[15]. To produce the *YUCB::GFPGUS* reporter construct pMT244 (Figure S3), a 2090 bp *YUCB* promoter fragment was amplified from gDNA with primers SS235/SS236 and trimmed with *Bam*HI/*Nco*I. The resulting fragment was cloned between the *Bam*HI/*Nco*I sites of pMT211, a vector allowing promoters to be cloned ahead of a GFP-GUS reporter gene for subsequent integration into the neutral *Pp108* locus[45]. Similarly, to produce the *YUCC::GFPGUS* reporter construct pMT251 (Figure S3), a 1767 bp *YUCC* promoter fragment was amplified from gDNA with primers SS237/SS238, trimmed with *Bam*HI/*Bsp*HI, and cloned between the same two sites in pMT211. Both reporter constructs were linearized with *Sfi*I before they were transformed into WT protoplast as previously described[46]. Stable transformants were selected in the presence of 50 μg.ml^{-1} hygromycin (Duchefa H0192; Haarlem, the Netherlands). Correct integration was confirmed by PCR (Figure S3). For primer sequences, see Table S5. The *yuccf* double knockout lines were produced by a sexual cross of the confirmed single mutants *Ppyucc-2* and *Ppyucf-1* described previously[15], according to the method presented in Thelander *et al*.[45]. Double knockout lines were confirmed by PCRs demonstrating the loss of internal gene sequences (Figure S5).

GUS staining and plant imaging

Physcomitrium patens gametophores were isolated from colonies grown on BCDAT and incubated at 37°C in a 100 mM phosphate buffer (pH 7) with 10 mM Tris (pH 8), 1 mM EDTA (pH 8), 0.05% Triton X-100, 5mM potassium ferricyanide, 5mM potassium ferrocyanide and 2 mM X-GlcA (5-Bromo-4-chloro-3-indolyl-β-D-glucuronic acid), using times indicated in Figure 2. Tissues were de-stained in 70% ethanol and imaged with a Keyence VHX-900F digital microscope with a 5-50 X or a 50-200 X objective. Two to three independent transgenic lines were observed for each genetic construct (Table S4). Plants not subject to GUS staining were imaged in the same conditions.

Definition of branches in *Physcomitrium patens*

According to Coudert *et al.*[11], a module is defined as “a portion of gametophore arising from a single apical cell”. Here, we consider that the main gametophore axis corresponds to a Class I module, and gametophore branches correspond to Class II lateral modules.

RNA-seq data production and analysis

For each biological replicate and condition, RNA were pooled from 5-10 gametophores (Gransden[47] strain). Three independent biological replicates were produced. Total RNA was extracted using a RNeasy Plant Mini Kit (Qiagen, Hilden, Germany) and treated with DNase

according to the supplier's instructions. RNA-seq libraries were made using the TruSeq_Stranded_mRNA_SamplePrep_Guide_15031047_D protocol (Illumina, California, U.S.A.). The RNA-seq samples have been sequenced in paired-end (PE) with a sizing of 260 bp and a read length of 75 bases, using an Illumina NexSeq500 technology (IPS2, POPS platform, Gif-sur-Yvette). 24 samples were processed by lane of NextSeq500 using individual bar-coded adapters, generating approximately 30 million of PE reads per sample. All experimental steps, from growth conditions to bioinformatic analyses, were deposited in the CATdb database[48] (http://tools.ips2.u-psud.fr/CATdb/, ProjectID NGS2017_09_Moss1) according to the MINSEQE 'minimum information about a high-throughput sequencing experiment' (https://doi.org/10.25504/FAIRsharing.a55z32). To facilitate comparisons, all samples were processed similarly from trimming to count. RNA-Seq pre-processing included trimming library adapters and performing quality controls. Raw data (fastq) were trimmed with fastx toolkit for Phred Quality Score Qscore >20, read length >30 bases, and ribosome sequences were removed with sortMeRNA[49]. The mapper Bowtie[50] (version 2) was used to align reads against the *Physcomitrium* (*Physcomitrella*) *patens* transcriptome (with local option and other default parameters). The 32926 genes were extracted from Phytozome database (*Physcomitrella patens* transcripts v3.1 gene model). The abundance of each gene was calculated by a local script which parses SAM files and counts only paired-end reads for which both reads map unambiguously one gene, removing multi-hits. According to these rules, around 82,7% of PE reads were associated to a gene, 5-6% PE reads were unmapped and 12-13% of PE reads with multi-hits were removed. Choices for the differential analysis were made based on the article by Rigaill *et al*[51]. Genes which did not have at least one read after a counts per million (CPM) normalization in at least one half of the samples were discarded. Library size was normalized using the TMM method and count distribution was modeled with a negative binomial generalized linear model. Dispersion was estimated by the edgeR method[52] (version 1.12.0) in the statistical software 'R' (http://www.R-project.org, version 2.15.0). Expression differences were compared between "0 h.a.d." and "2 h.a.d.", "6 h.a.d.", "12 h.a.d." or "24 h.a.d." conditions for the "decapitation experiment", and between samples "mock" and "10µM IAA" conditions for the "auxin experiment", using likelihood ratio test and p-values were adjusted by the Benjamini-Hochberg procedure to control FDR. A gene was considered as differentially expressed if its adjusted p-value was lower than 0.05. Venn diagrams were generated using InteractiVenn[53]. Gene Ontology (GO) term enrichment analyses were performed with ShinyGO (version 0.66)[54].

RNA-seq data availability

RNA-seq datasets are available in the international repository GEO (Gene Expression Omnibus[55], http://www.ncbi.nlm.nih.gov/geo) under the project identifier GSE188843.

Gene identifiers

Gene identifiers were obtained from the most recent annotation (version 3.3) of *P. patens* genome[56]. Identifiers of *PpIAA* and *PpARF* genes (Figure 1) are : *PpIAA1B*, *Pp3c8_14720* ; *PpIAA2*, *Pp3c24_6610* ; *PpARFa1*, *Pp3c1_14480* ; *PpARFa3*, *Pp3c2_25890* ; *PpARFa4*, *Pp3c13_4720* ; *PpARFa5*, *Pp3c26_11550* ; *PpARFa6*, *Pp3c17_19900* ; *PpARFa7*, *Pp3c14_16990* ; *PpARFa8*, *Pp3c1_40270* ; *PpARFb1*, *Pp3c27_60* ; *PpARFb2*, *Pp3c16_6100* ; *PpARFb3*, *Pp3c5_9420* ; *PpARFb4*, *Pp3c6_21370* ; *PpARFc1B*, *Pp3c4_13010* ; *PpARFc2*, *Pp3c6_26890* ; *PpARFd1*, *Pp3c9_21330* and *PpARFd2*, *Pp3c15_9710*. Identifiers of *PpTAR* and *PpYUC* genes (Figure 1) are : *PpTARA*, *Pp3c21_15370* ; *PpTARB*, *Pp3c18_15140* ; *PpTARC*, *Pp3c17_6500* ; *PpTARD*, *Pp3c26_12520* ; *PpYUCA*, *Pp3c3_18590* ; *PpYUCB*, *Pp3c11_11790* ; *PpYUCC*, *Pp3c1_11500* ; *PpYUCD*, *Pp3c2_27740* ; *PpYUCE*, *Pp3c13_21970* and *PpYUCF*, *Pp3c3_20490*.

Quantitative RT-PCR

For expression analyses, apices (including the apical cell and a few phyllids) and newly emerged branches (same stages as in Figure 2H-I, K-L, N-O) were dissected out with micro-scissors and thin tweezers from intact and decapitated gametophores, respectively. Total RNA was isolated using the INVITROGEN PureLink™ RNA Mini Kit (Ref: 12183025). RNA was DNase treated with ezDNase™ enzyme prior to reverse transcription with SuperScript™ IV VILO™ Master Mix (Ref: 11766050) following manufacturer's guidelines. qRT-PCR was performed using a ROCHE Fast Start Universal SYBR Green master mix and a ThermoFisher StepOnePlus Real-Time PCR System. Thermocycling conditions were: 95°C 10 min; 95°C 10 sec, 58°C 30 sec (40 cycles). Specificity of PCR amplification was checked by melt curve analysis at each run. *PpTARA*, *PpTARC, PpYUCB, PpYUCC, PpYUCF* and *PpUBI* genes were respectively amplified using the following primer pairs: YCL-R1-TARA-144F, YCL-R1-TARA-144R, YCL-R1-TARC-145F, YCL-R1-TARC-145R, YCL-R1-YUCB-146F, YCL-R1-YUCB-146R, YCL-R1-YUCC-147F, YCL-R1-YUCC-147R, YCL-R1-YUCF-148F, YCL-R1-YUCF-148R, YCL-12F-R1-UBI and YCL-12R-R1-UBI. Expression level of *PpUBI* (Pp1s56_52V6.1, Pp3c12_5760V3.1) was used as a reference to normalize gene expression level between conditions, and Ct values were converted into relative expression values using the comparative Ct method[57].

Sample-size estimation and replicates

For data shown in Figure 1, three independent biological replicates were produced for each condition, and each replicate corresponded to RNA extracted from 5 to 10 gametophores. For Figure 2, two or three independent transgenic lines were analysed for *TAR* and *YUC* transcriptional reporters. Independent lines transformed with the same genetic construct showed similar GUS staining patterns. Numbers in panels A, D, G, J and M indicate the proportion of gametophores with a GUS staining pattern similar to the picture. For Figure 3, data shown in panels A-D were obtained from 60 gametophores collected 5-7 weeks after protonema inoculation, data in panels K and L correspond to all gametophores, and metrics in panels M, N and P could be calculated only for gametophores with more than one branch. For Figure S9, data shown in panels A-C, E-F, I-J were obtained from 60 gametophores collected 5-9 weeks after protonema inoculation.

Statistical analyses

Significance of association between IAA repression/induction and decapitation repression/induction was assessed via chi-squared tests. Generalised linear modelling was used to test whether the relationship between branch number and gametophore length depended on genotype (File S1). Poisson or negative binomial regression was used, depending on whether the data were over-dispersed, *i.e.* whether the data were more variable than would be expected under a Poisson model. The most complex fitted models were of the form $\log(\mathbb{E}(B|L,X)) = a_0 + a_1X + (a_2 + a_3X)L$, in which a_0, a_1, a_2 and a_3 are coefficients, L is the length, X is an indicator variable depending on genotype (*i.e.* X took values of either 0 or 1 depending upon whether the mutant or WT was considered), and $\mathbb{E}(B|L,X)$ is the expected branch number (B) at any given pair of values of L and X. Analysis of deviance and backwards stepwise elimination was used to find the minimal model that received support from the experimental data. A mutant was considered different from WT if either the interaction term (a_3) or the term corresponding to genotype (a_1) remained in the minimal model, *i.e.* if the expected branch number was affected by the value of X. The choice of whether to use a Poisson and negative binomial model was made via a formal test of over-dispersion for the Poisson version of the model with an interaction, using the function overdispersion() in the package AER[58]. The terms “weak”, “moderate”, “strong” and “very strong evidence” reflected the translation of p-values into the language of evidence proposed by Muff *et al*.[59]

Figures and figure legends

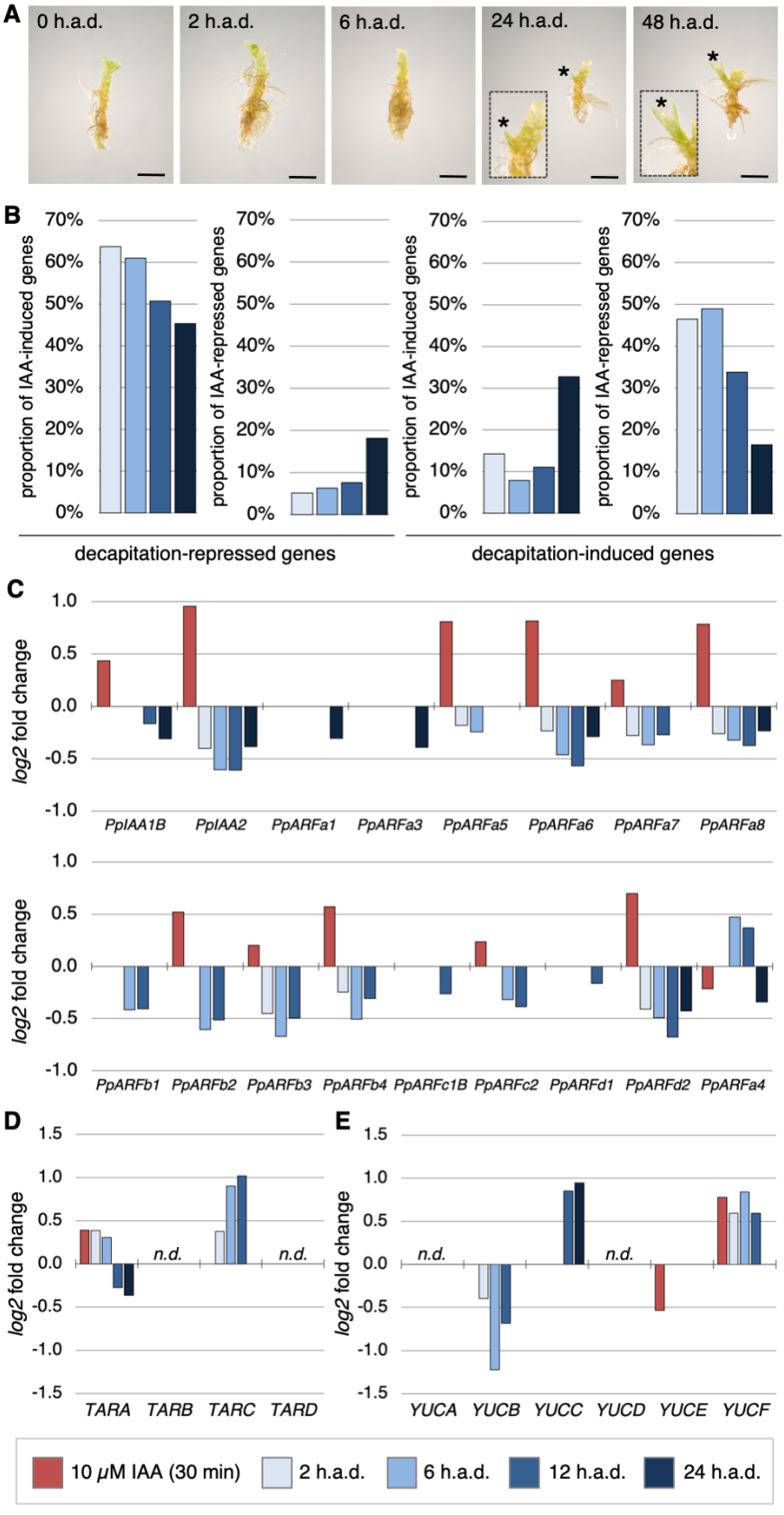

Figure 1. Decapitation and auxin treatment have opposite effects on auxin-responsive and auxin signalling gene expression, and affect auxin biosynthesis gene activity in moss gametophores. (**A**) New branches (indicated with asterisks) emerged within 24 hours after gametophore decapitation. Leaves were removed before imaging to observe gametophore branches. Insets show magnifications of emerging branches. Scale bar = 1 mm. (**B**) Cross-analysis of transcriptomes of decapitated and auxin-treated gametophores showed that about two thirds of the genes repressed 2 h.a.d. were induced by a 30-minute treatment with 10 μM indole-3-acetic acid (auxin), and conversely nearly half of the genes induced 2 h.a.d. were repressed by auxin. (**C**) Bar plots showed that most *PpARF* and *PpIAA* auxin signalling genes identified were repressed after decapitation and induced by auxin. (**D-E**) Expression of two *TAR* and three *YUC* auxin biosynthesis genes was affected by decapitation. The colour code shown at the bottom of the figure is used in panels B-E. "*n.d.*" means not detected in the differential gene expression analysis.

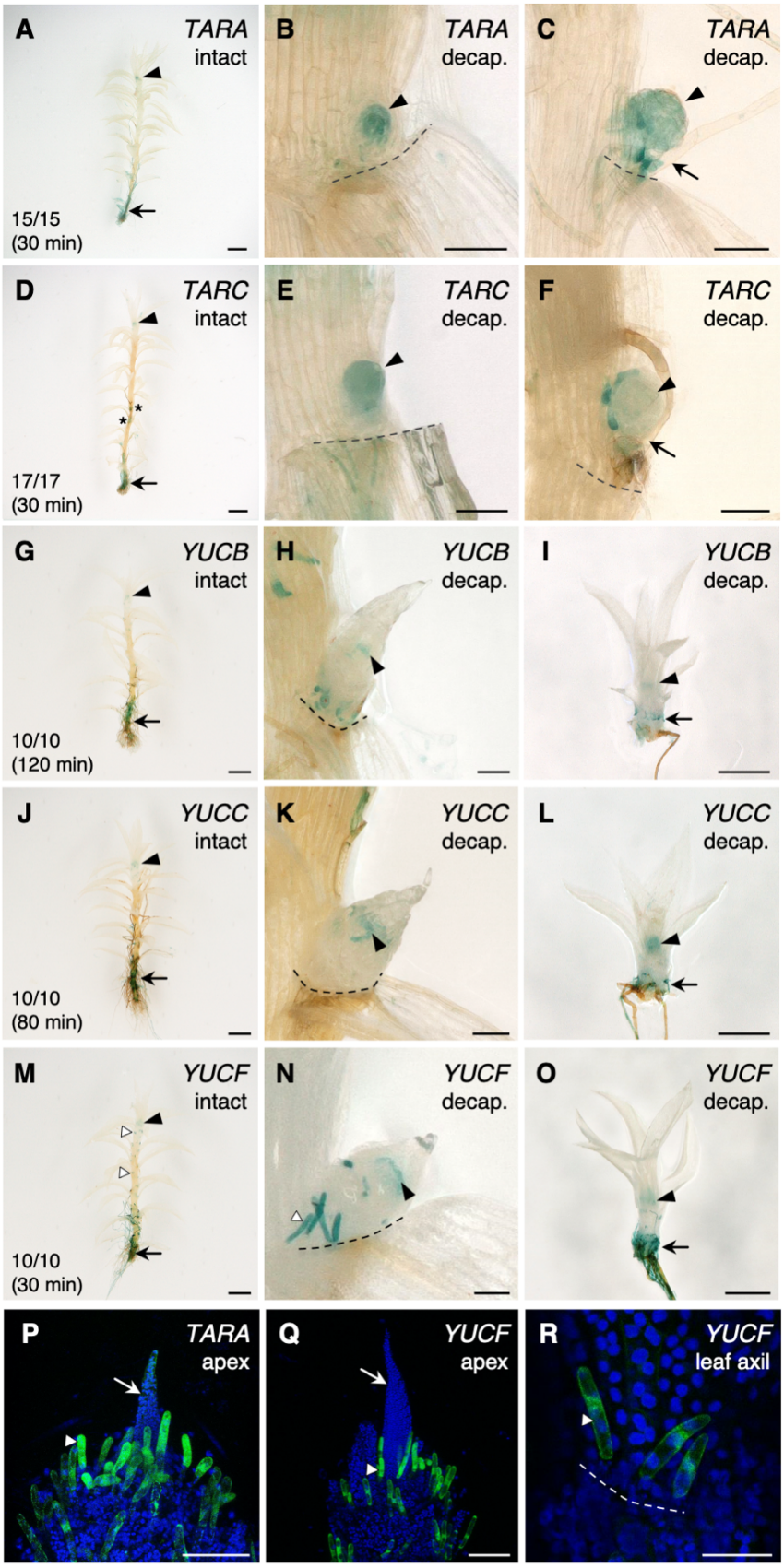

Figure 2. ***TAR*** **and** ***YUC*** **genes are expressed in meristematic and basal regions of** ***P. patens*** **gametophores**. (**A-O**) GUS staining of *TARA::GFP-GUS* (A-C), *TARC::GFP-GUS* (D-

F), *YUCB::GFP-GUS* (G-I), *YUCC::GFP-GUS* (J-L) and *YUCF::GFP-GUS* (M-O) transgenic lines revealed that *TAR* and *YUC* genes are active in largely overlapping expression domains. Gametophore were either observed before ("intact") or after ("decap.") apex excision. In intact gametophores, *TARA* and *TARC* are expressed in the main apex (black arrowheads), in emerging branches (asterisks) and in the basal region (black arrows) (A, D). Following decapitation, *TARA* and *TARC* expression is detected in initiating lateral branches (black arrowheads) but not in rhizoids (black arrows) (B, C, E, F). In intact gametophores, *YUCB*, *YUCC* and *YUCF* are expressed in the main apex (black arrowheads) and in the basal region (black arrows). *YUCF* expression is also observed in axillary hairs in leaf axils (white arrowheads) (G, J, M). Following decapitation, *YUCB*, *YUCC* and *YUCF* expression is first detected at a later stage than *TARA* and *TARC*. GUS staining was found in axillary hairs at the apex of newly formed branches (black arrowheads) and, at a later stage, in branch rhizoids (black arrows) (H, I, K, L, N, O). (**P-R**) GFP signal in *TARA::GFP-GUS* and *YUCF::GFP-GUS* lines was strongest in hairs (white arrowheads) located at the gametophore apex (P-Q), and/or in leaf axils (R). Emerging leaves are indicated with white arrows. Dashed lines mark the boundary between the stem and the detached leaf (B, C, E, F, H, K, N, R). Gametophores were soaked in GUS staining solution for times specified in panels A, D, G, J and M. The scale bars represent 1 mm in A, D, G, J and M, 500 μm in I, L, and O, 100 μm in B, C, E, F, H, K, P and Q, and 50 μm in N and R.

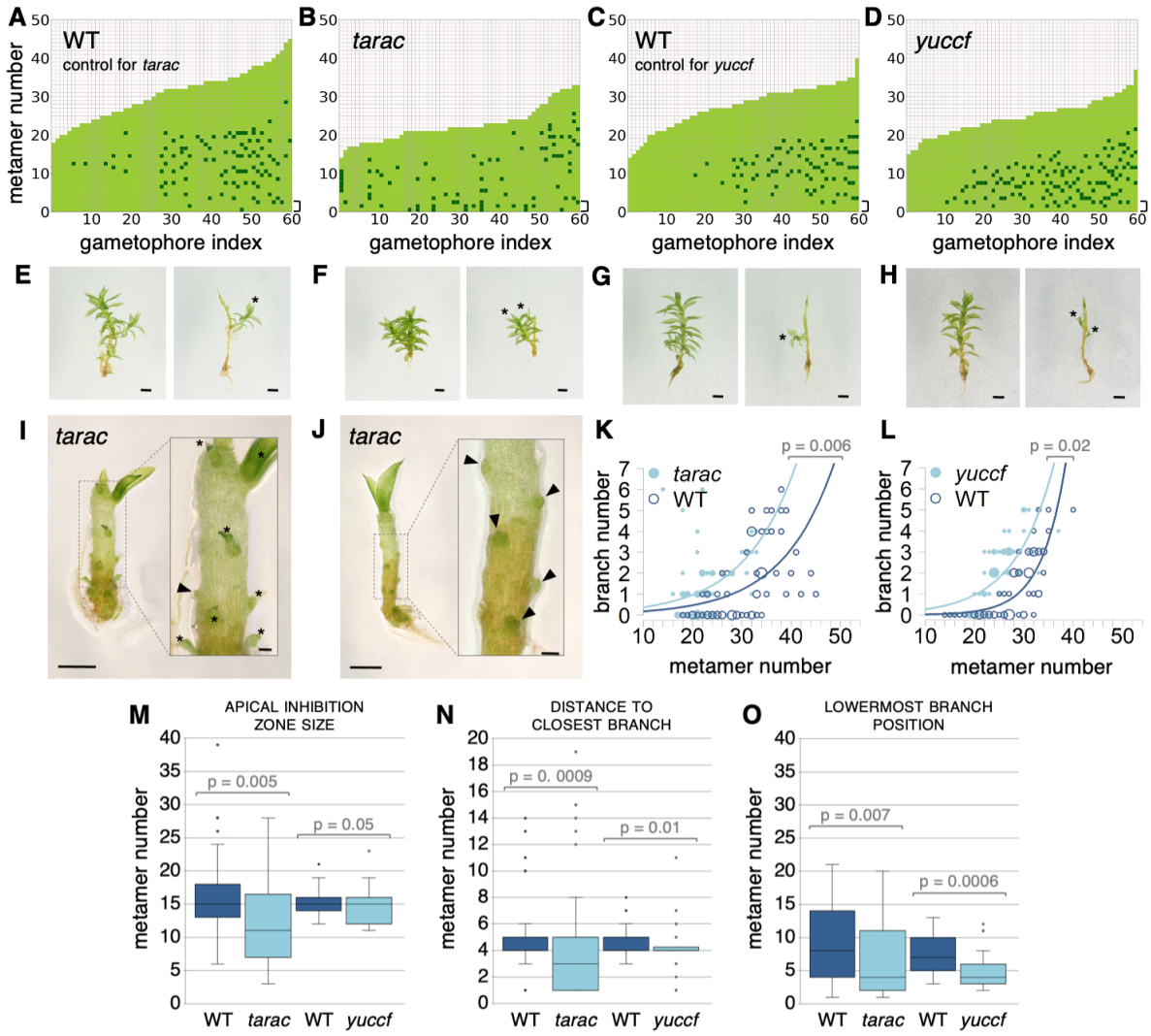

Figure 3. ***TAR* and *YUC* genes inhibit branch initiation, but *TAR* genes promote branch outgrowth**. (**A-D**) Plots show the branching patterns of 60 gametophores ordered by increasing size in *tarac* and *yuccf* double mutants, and corresponding wild-type (WT) controls. Each gametophore is represented as a series of metamers (light green squares) and lateral branch position is indicated in dark green. Brackets indicate the three lowermost metamers. (**E-H**) WT (E), *tarac* (F), WT (G) and *yuccf* (H) gametophores before (left) and after (right) removing leaves, with asterisks marking branches. Scale bars represent 1 mm. (**I-J**) *tarac* gametophores with leaves removed revealed dormant or arrested buds with no visible leaves (arrowheads) and tiny branches with few visible leaves (asterisks), which is never observed in WT in which branches initiate and immediately grow out. Scale bars represent 500 μm in the main panels and 100 μm in the insets. (**K-L**) Gametophore length is represented as the number of metamers and the bubble area is proportional to the number of gametophores with the same branch number (B) at a given length (L). Bubble plots showed that branch number at a given length is increased in *tarac* compared with WT. The data were over-

dispersed, and so negative binomial regression was used to test whether and how the relationship between branch number and gametophore length differed between mutants and WT (see 'Material and methods'). For (K) the best-fitting relationship indicated WT was smaller than *tarac* at all lengths (p-value=0.006; $\log(\mathbb{E}(B|L,W)) = -1.94 - 0.73W + 0.095L$, where $W = 1$ for WT). For *yuccf* mutants, the data were not over-dispersed, and so Poisson regression was used to test whether and how the relationship between branch number and gametophore length depended on treatment (see 'Material and methods' and SI data). The best-fitting relationship included an interaction, indicating the nature of the difference in the number of branches between WT and mutants depended upon the length (in (L), p = 0.02, $\log(\mathbb{E}(B|L,Y)) = -5.28 + 3.25Y + (0.20 - 0.08Y)L$, where $Y = 1$ for *yuccf*). (**M**) There was strong and moderate evidence that the apical inhibition zone was reduced in *tarac* and *yuccf* double mutants, respectively, compared with corresponding wild-type controls (Wilcoxon rank sum test with continuity correction; WT versus *tarac*, p-value = 0.005; WT versus *yuccf*, p-value = 0.05). (**N**) There was very strong and strong evidence that the distance to the closest branch, a measurement of branch spacing, was reduced in *tarac* and *yuccf* double mutants, respectively, compared with wild-type controls (Wilcoxon rank sum test with continuity correction; WT versus *tarac*, p-value = 0.0009; WT versus *yuccf*, p-value = 0.01). (**O**) There was very strong evidence that the position of the lowermost branch was closer to the gametophore base in *tarac* and *yuccf* double mutants than in WT (Wilcoxon rank sum test with continuity correction; WT versus *tarac*, p-value = 0.007; WT versus *yuccf*, p-value = 0.0006). The terms "weak", "moderate", "strong" and "very strong evidence" reflected the translation of p-values into the language of evidence proposed by Muff *et al*.[59]

492 **Supplementary data**

493

494

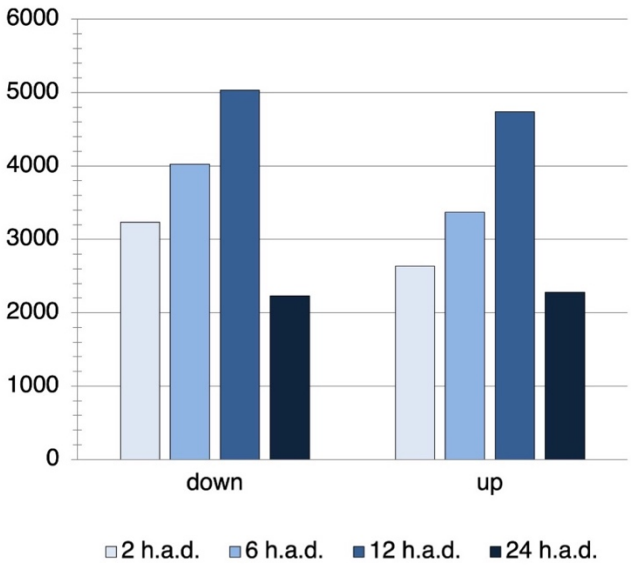

495

496 **Figure S1. Number of genes repressed or induced 2, 6, 12 and 24 hours after**
497 **decapitation.**

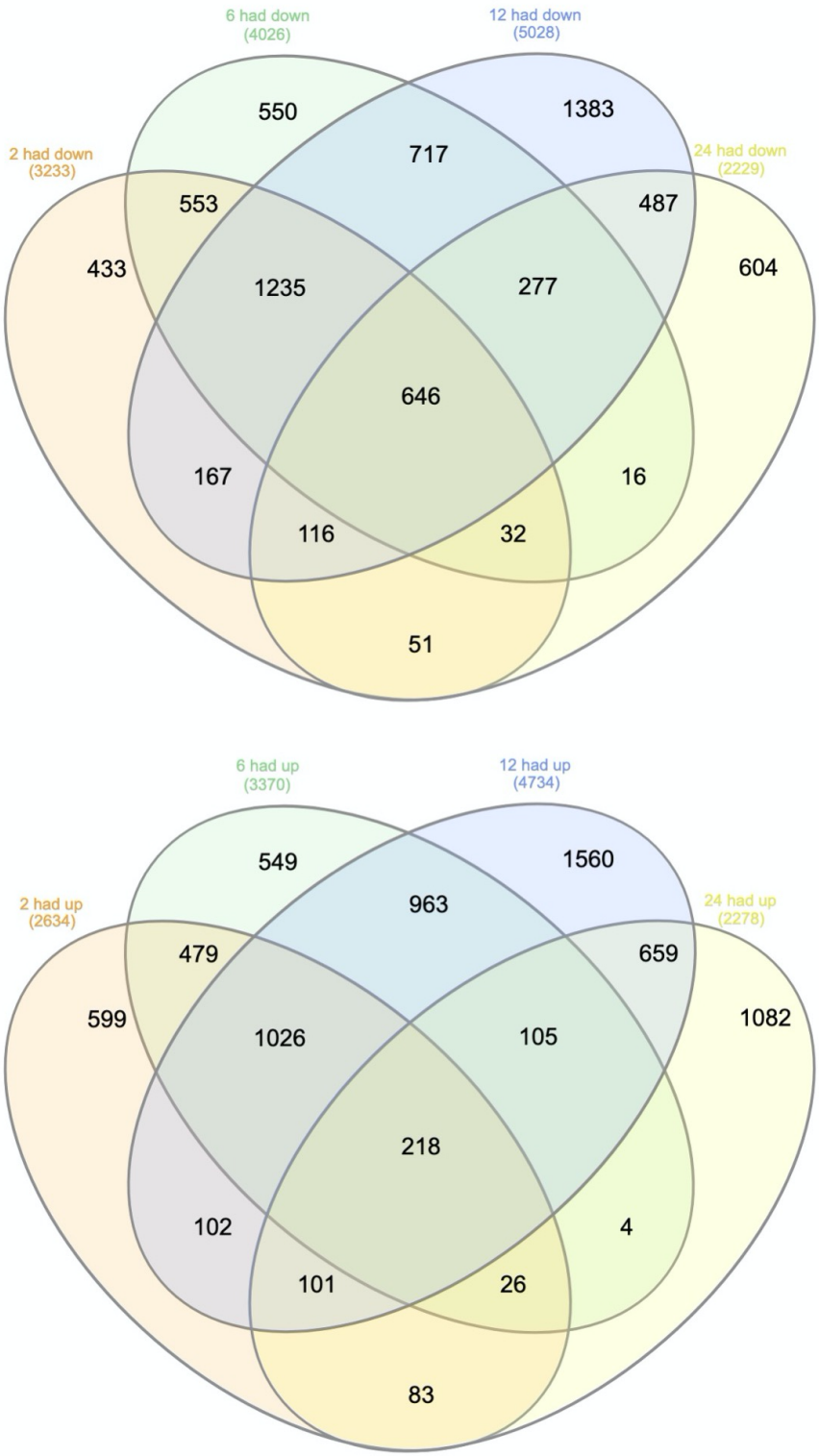

Figure S2. Venn diagrams for all genes repressed or induced 2, 6, 12 and 24 hours after decapitation.

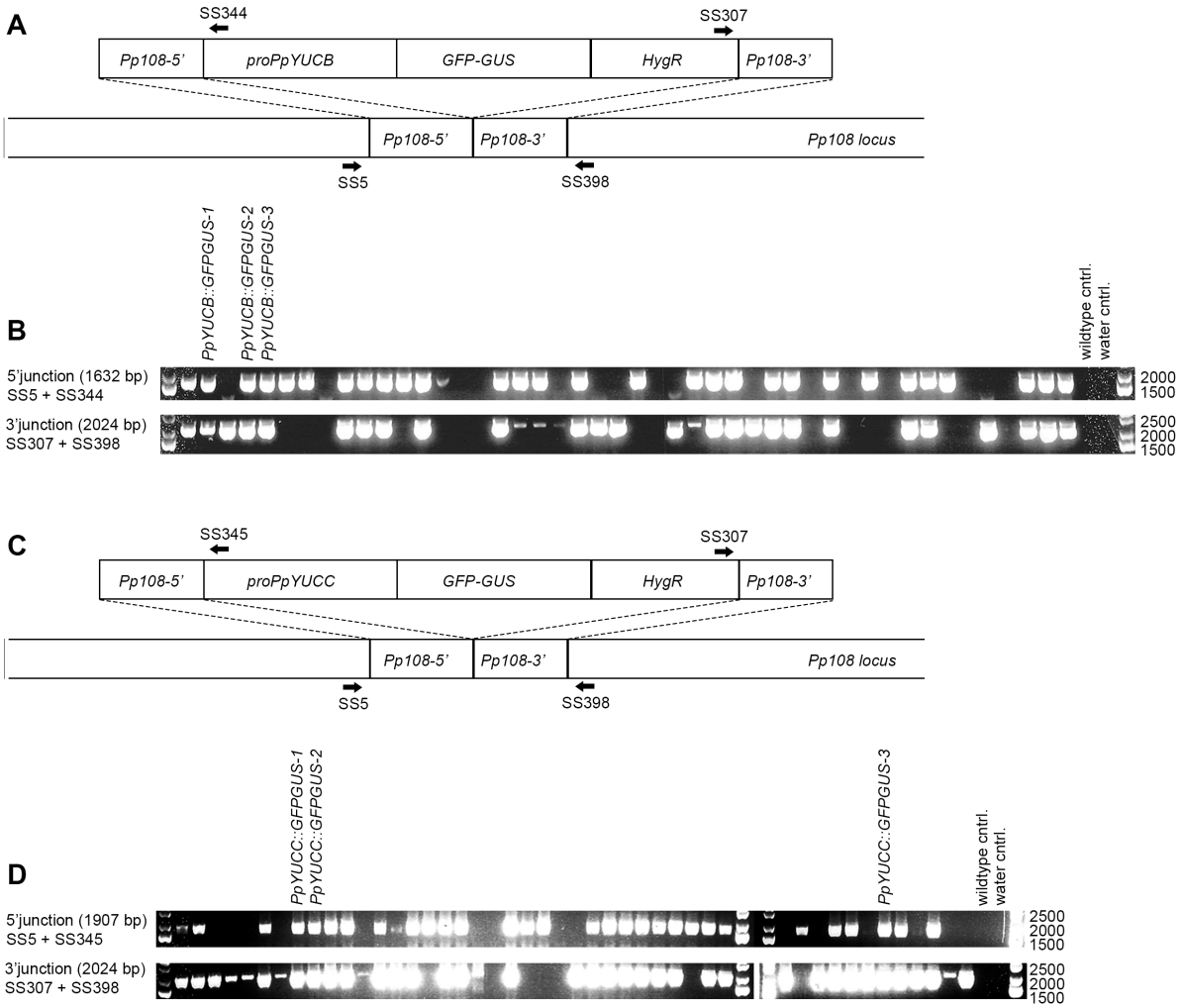

Figure S3. PCR verification of *PpYUCB and PpYUCC* transcriptional reporter lines in WT background (**A**) Schematic view of the *PpYUCB::GFPGUS* reporter construct pMT244 and the *Pp108* locus to which it was targeted. Arrows mark the approximate annealing sites of primers used for PCR verification in B. (**B**) PCR verification of 5' and 3' junctions to confirm correct integration of the *PpYUCB::GFPGUS* reporter construct into the Pp108 locus. (**C**) Schematic view of the *PpYUCC::GFPGUS* reporter construct pMT251 and the *Pp108* locus to which it was targeted. Arrows mark the approximate annealing sites of primers used for PCR verification in D. (**D**) PCR verification of 5' and 3' junctions to confirm correct integration of the *PpYUCC::GFPGUS* reporter construct into the Pp108 locus. In both B and D, expected product sizes are indicated within parentheses. For primer sequences, see Table S5.

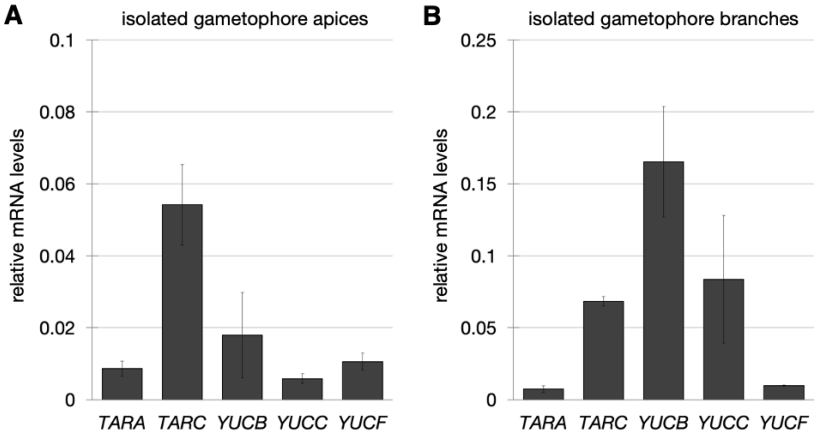

516
517

518 **Figure S4. Quantitative RT-PCR analysis of *TARA*, *TARC*, *YUCB*, *YUCC* and *YUCF***
519 **mRNA accumulation levels relative to *UBI* internal control in *Physcomitrium patens***
520 **gametophore apices (A) and branches (B)** (mean level of three independent biological
521 replicates ± SD).

522

523

524

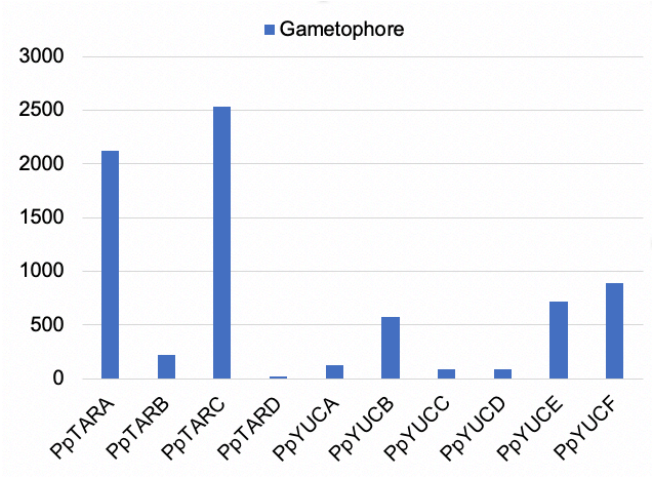

Figure S5. Absolute expression levels of *TAR* and *YUC* genes in *P. patens* gametophores retrieved from Ortiz-Ramirez *et al*. (2016)[60]. Correspondence between gene names and identifiers: *PpTARA* (Pp3c21_15370V3.1, Pp1s167_103V6.1), *PpTARB* (Pp3c18_15140V3.1, Pp1s3_273V6.1), *PpTARC* (Pp3c17_6500V3.1, Pp1s26_28V6.1), *PpTARD* (Pp3c26_12520V3.1, Pp1s6_329V6.1), *PpYUCA* (Pp3c3_18590V1.1, Pp1s312_60V6.1), *PpYUCB* (Pp3c11_11790V3.1, Pp1s11_6V6.1), *PpYUCC* (Pp3c1_11500V3.1, Pp1s139_131V6.1), *PpYUCD* (Pp3c2_27740V3.1, Pp1s22_291V6.1), *PpYUCE* (Pp3c13_21970V3.1, Pp1s37_90V6.1), *PpYUCF* (Pp3c3_20490V3.1, Pp1s204_126V6.1).

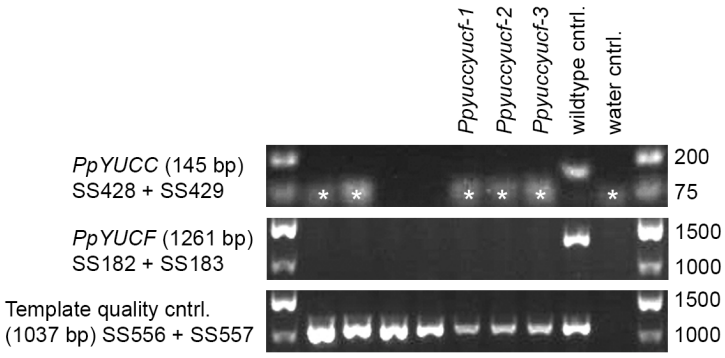

538

539

540 **Figure S6. PCR genotyping of *yuccf* double knockout lines produced by a sexual cross**
541 **of the single knockout lines *Ppyucc-2* and *Ppyucf-1*** (Landberg et al., 2020)[15]. The upper
542 panel shows the result for a PCR confirming the loss of an internal *PpYUCC* gene sequence.
543 Asterisks mark primer dimers. The middle panel shows the result for a PCR confirming the
544 loss of an internal *PpYUCF* gene sequence. The bottom panel shows amplification of an
545 unrelated locus to confirm integrity of the gDNA used as template in all three panels. Next to
546 each panel, the primers used and the expected product size are noted. For primer sequences,
547 see Table S5.

548

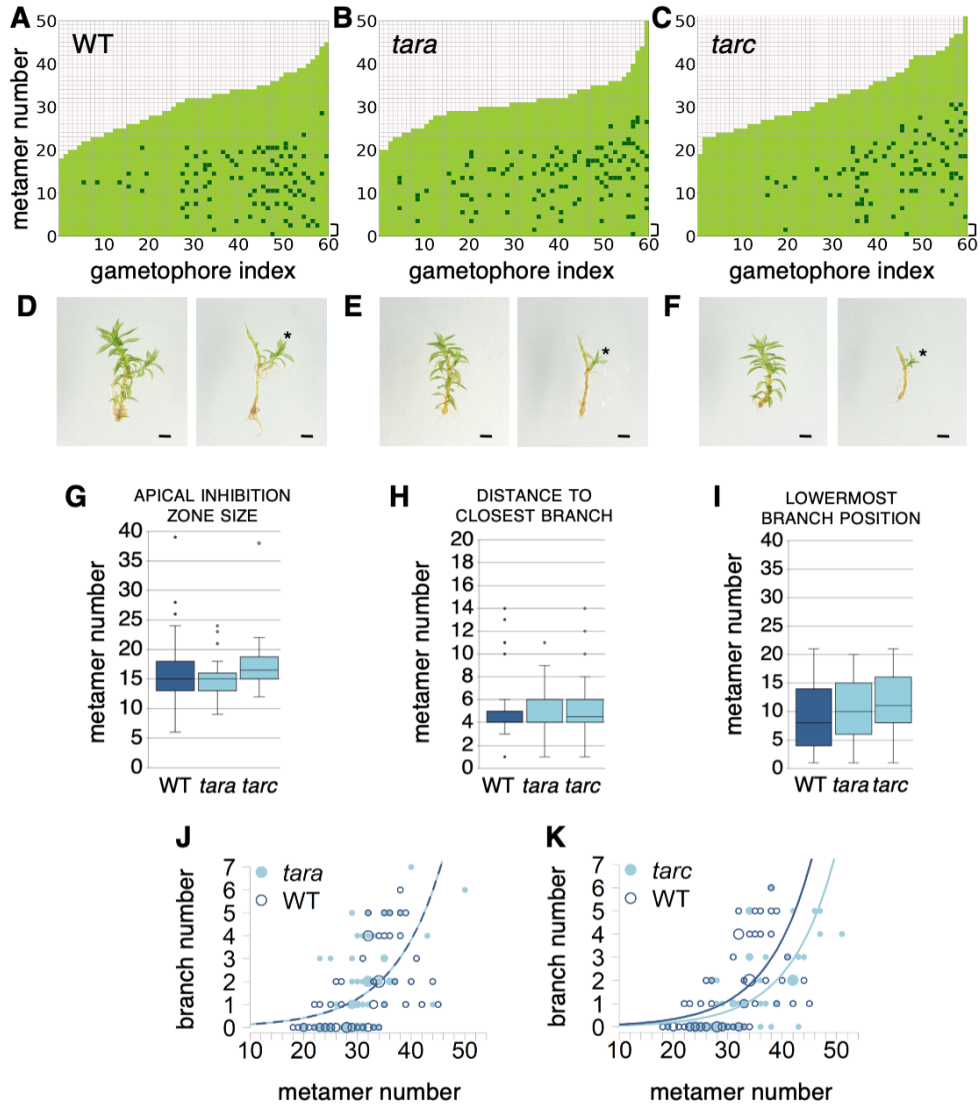

549

550 **Figure S7**. ***tara*** **and** ***tarc*** **mutants have similar gametophore branching patterns than**
551 **wild-type**. (**A-C**) Branching patterns in wild-type (WT), *tara* and *tarc* gametophores. Brackets
552 indicate the three lowermost metamers. (**D-F**) WT (D), *tara* (E) and *tarc* (F) gametophores
553 before (left) and after (right) removing leaves, with asterisks marking branches. Scale bars
554 represent 1 mm. (**G**) The apical inhibition zone was not different in *tara* or *tarc* single mutants,
555 compared with wild-type control (Wilcoxon rank sum test with continuity correction; WT
556 versus *tara*, p-value = 0.35 ; WT versus *tarc*, p-value = 0.07). (**H**) The distance to the closest
557 branch was not different in *tara* or *tarc* single mutants, compared with wild-type control
558 (Wilcoxon rank sum test with continuity correction; WT versus *tara*, p-value = 0.92 ; WT
559 versus *tarc*, p-value = 0.14). (**I**) The position of the lowermost branch was similar in *tara*, *tarc*
560 and WT (Wilcoxon rank sum test with continuity correction ; WT versus *tara*, p-value = 0.30 ;
561 WT versus *tarc*, p-value = 0.12). (**J-K**) Bubble plots showed that branch number at a given
562 length slightly decreased in older *tarc* gametophores and unchanged in *tara*, compared with

WT. Gametophore length is represented as the number of metamers and the bubble area is proportional to the number of gametophores with the same branch number (B) at a given length (L). The data were over-dispersed, and so negative binomial regression was used to test whether and how the relationship between branch number and gametophore length differed between mutants and WT. For (J) the best-fitting relationship indicated no difference between *tara* and WT (p-value = 0.39; $\log(\mathbb{E}(B|L)) = -3.11 + 0.11L$ for both treatments). For (K) the best-fitting relationship indicated WT was larger than *tarc* at all lengths (p-value = 0.01; $\log(\mathbb{E}(B|L,W)) = -4.02 + 0.50W + 0.12L$, where $W = 1$ for WT). Data for WT were replicated from Figure 3.

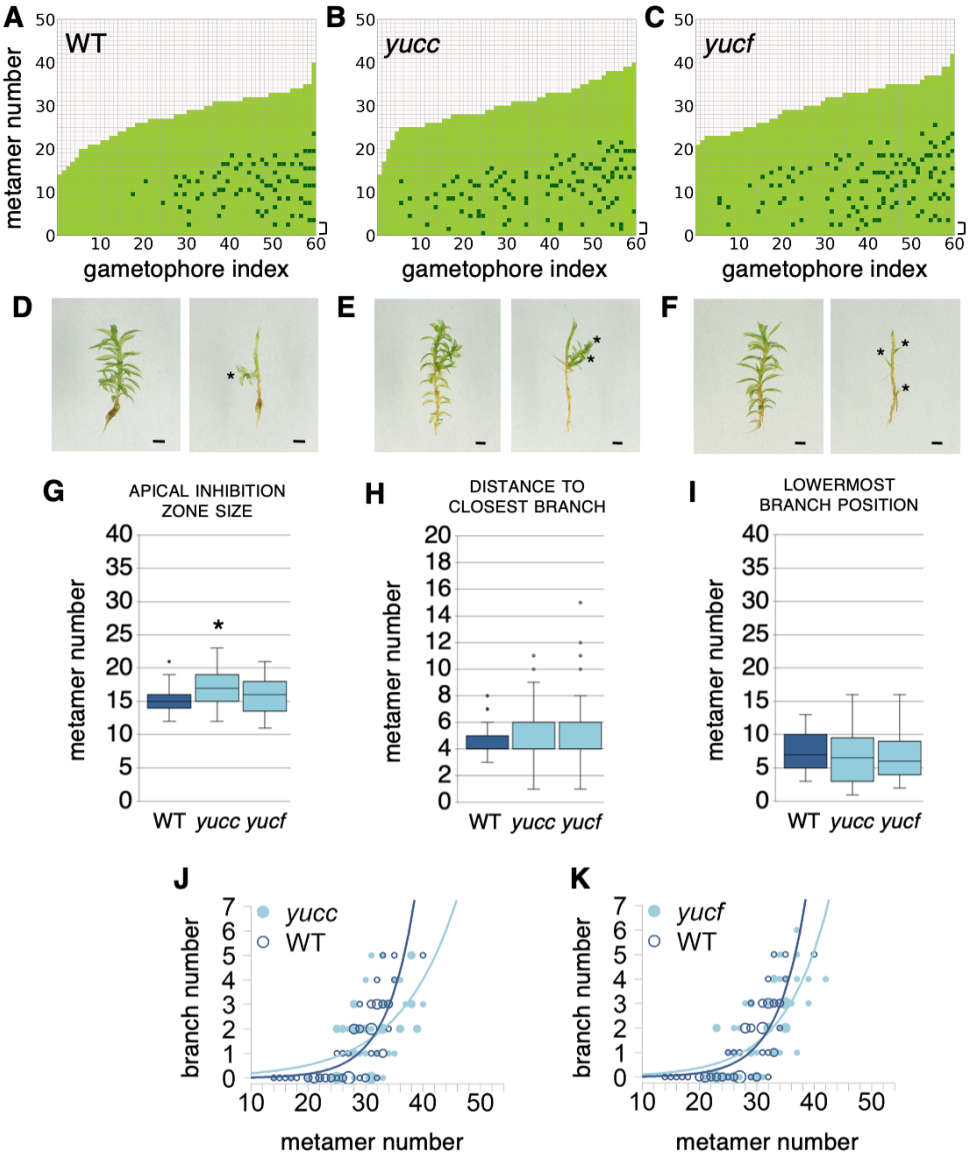

Figure S8. ***yucc* and *yucf* mutant gametophores have only minor perturbations in their branching patterns**. (**A-C**) Branching patterns in WT, *yucc* and *yucf* mutants. Brackets indicate the three lowermost metamers. (**D-F**) WT (E), *yucc* (F) and *yucf* (G) gametophores before (left) and after (right) removing leaves, with asterisks marking branches. Scale bars represent 1 mm. (**G**) The apical inhibition zone was increased in *yucc* mutants compared with wild-type control (Wilcoxon rank sum test with continuity correction different from WT, *p-value ≤ 0.05 ; WT versus *yucc*, p-value = 0.003 ; WT versus *yucf*, p-value = 0.82). (**H**) The distance to the closest branch was similar in *yucc* and *yucf* single mutants, compared with wild-type control (Wilcoxon rank sum test with continuity correction; WT versus *yuc*, p-value = 0.77 ; WT versus *yucf*, p-value = 0.76). (**I**) The position of the lowermost branch was similar in *yucc*, *yucf* and WT (Wilcoxon rank sum test with continuity correction; WT versus *yucc*, p-value = 0.49 ; WT versus *yucf*, p-value = 0.34). (**J-K**) Bubble plots showed that branch number

responded differently to length in all mutants compared with WT. Gametophore length is represented as the number of metamers and the bubble area is proportional to the number of gametophores with the same branch number (B) at a given length (L). The data were not over-dispersed, and so Poisson regression was used to test whether and how the relationship between branch number and gametophore length depended on treatment (see 'Material and methods'). The best-fitting relationship included an interaction for all three mutants, indicating the nature of the difference in the number of branches between WT and mutant depended upon the length (in (J), p = 0.002, $\log(\mathbb{E}(B|L,Y)) = -5.28 + 3.17Y + (0.20 - 0.10Y)L$, where $Y = 1$ for *yucc*; in (K) p = 0.03, $\log(\mathbb{E}(B|L,Y)) = -5.28 + 2.25Y + (0.20 - 0.07Y)L$, where $Y = 1$ for *yucf*). Data for WT were replicated from Figure 3.

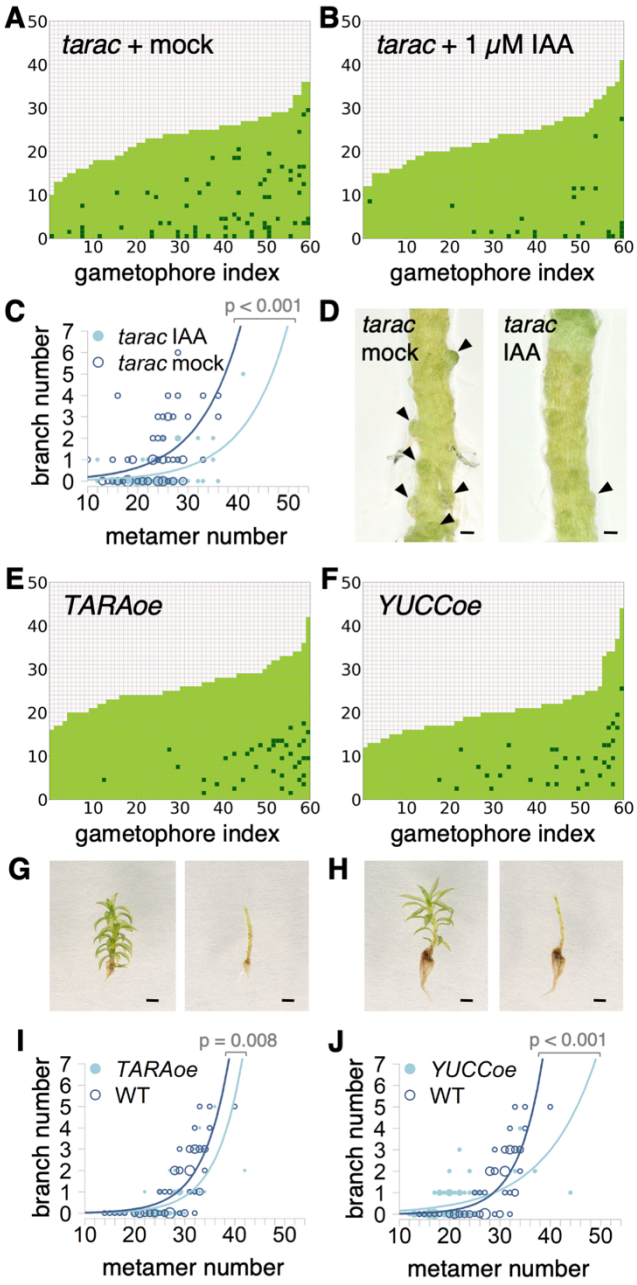

Figure S9. ***tarac*** **double mutants treated with auxin, and** ***TARA*** **and** ***YUCC*** **overexpression lines have reduced gametophore branching**. (**A-B**) Plots show the branching patterns of 60 gametophores in *tarac* double mutants treated with solvent control (A) or 1 μM IAA (B). Each gametophore is represented as a series of metamers (light green squares) and lateral branch position is indicated in dark green. (**C**) Gametophore length is represented as the number of metamers and the bubble area is proportional to the number of gametophores with the same branch number (B) at a given length (L). Data were not over-dispersed, and so Poisson regression was used to test whether and how the relationship between branch number and gametophore length depended on treatment. For *tarac*, the

608 best-fitting relationship indicated *tarac* + mock was larger than *tarac* + IAA at all lengths (p-
609 value < 0.001; log($\mathbb{E}(B|L$, W)) = -3.93 + 1.11M + 0.19L, where M = 1 for *tarac* + mock). (**D**)
610 Mock-treated *tarac* gametophores had numerous arrested axillary buds (arrowheads), this
611 phenotype was largely suppressed by IAA treatment. Leaves were removed prior to imaging.
612 Scale bars represent 100 μm. (**E-F**) Plots show the branching patterns of 60 gametophores
613 ordered by increasing size in *TARA* (E) and *YUCC* (F) overexpression (oe) lines, corresponding
614 WT is shown in Figure 3C. (**G-H**) *TARAoe* (G) and *YUCCoe* (H) gametophores before (left) and
615 after (right) removing leaves. Scale bars represent 1 mm. (**I-J**) Data were not over-dispersed,
616 and so Poisson regression was used to test whether and how the relationship between
617 branch number and gametophore length depended on treatment. For *TARAoe*, the best-
618 fitting relationship indicated *TARAoe* was smaller than WT at all lengths (p-value =
619 0.008, log($\mathbb{E}(B|L$, W)) = –5.98 + 0.51W + 0.19L, where W = 1 for WT). For *YUCCoe*, the best-
620 fitting relationship included an interaction, indicating the nature of the difference in the
621 number of branches between WT and mutants depended on length (p-value <
622 0.001, *log($\mathbb{E}(B|L$, Y)) = –5.82 + 3.00Y + (0.20 – 0.10Y)L, where Y = 1 for YUCCoe*).
623

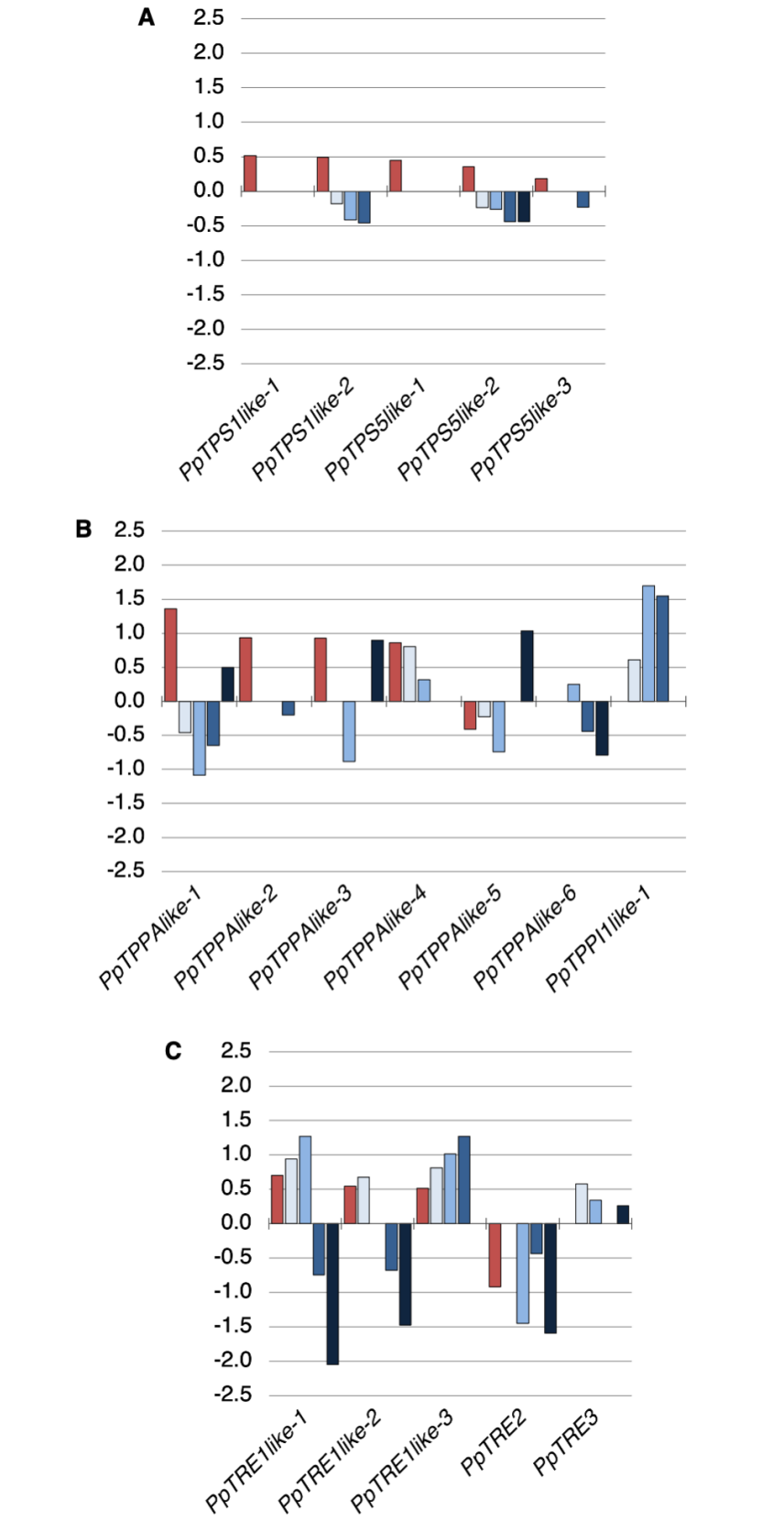
A
2.5
2.0
1.5
1.0
0.5
0.0
-0.5
-1.0
-1.5
-2.0
-2.5
PpTPS1like-1
PpTPS1like-2
PpTPS5like-1
PpTPS5like-2
PpTPS5like-3
B
PpTPPAlike-1
PpTPPAlike-2
PpTPPAlike-3
PpTPPAlike-4
PpTPPAlike-5
PpTPPAlike-6
PpTPP1like-1
C
PpTRE1like-1
PpTRE1like-2
PpTRE1like-3
PpTRE2
PpTRE3
2 h.a.d.
6 h.a.d.
12 h.a.d.
24 h.a.d.
10 μM IAA (30 min)

624

Figure S10. Expression of trehalose-6-phosphate (T6P) metabolism genes is affected by auxin and gametophore decapitation. Bar plots show *log2* fold-change in expression of *T6P synthase* (*PpTPS*), *T6P phosphatase* (*PpTPP*) and *trehalase* (*PpTRE*) coding genes in wild-type gametophores after treatment with auxin (red bars) or decapitation (blue bars). Correspondence between gene names and identifiers: *PpTPPAlike-1* (Pp3c12_20050V3.1), *PpTPPAlike-2* (Pp3c4_20080V3.1), *PpTPPAlike-3* (Pp3c4_11080V3.1), *PpTPPAlike-4* (Pp3c10_13170V3.1), *PpTPPAlike-5* (Pp3c3_25080V3.1), *PpTPPAlike-6* (Pp3c3_22990V3.1), *PpTPPC1like-1* (Pp3c12_7510V3.1), *PpTPPE1like-1* (Pp3c12_7530V3.1), *PpTPPI1like-1* (Pp3c10_23130V3.1), *PpTPS1like-1* (Pp3c5_17730V3.1), *PpTPS1like-2* (Pp3c6_16450V3.1), *PpTPS5like-1* (Pp3c25_6990V3.1), *PpTPS5like-2* (Pp3c11_17560V3.1), *PpTPS5like-3* (Pp3c7_15250V3.1), *PpTRE1like-1* (Pp3c5_16470V3.1), *PpTRE1like-2* (Pp3c23_11240V3.1), *PpTRE1like-3* (Pp3c16_7830V3.1), *PpTRE1like-4* (Pp3c24_9748V3.1), *PpTRE1like-5* (Pp3c24_9750V3.1), *PpTRE2* (Pp3c6_4940V3.1), *PpTRE3* (Pp3c10_5310V3.1). GO terms related to "trehalose metabolism" were significantly enriched in the "up-regulated 2 h.a.d." gene set (Table S2). Trehalose 6-phosphate (T6P) metabolic genes regulate branching and apical dominance in flowering plants. For example, shoot decapitation in *Pisum sativum* (pea) triggers an increase of T6P levels in a few hours, which contributes to promoting branch outgrowth[22]. T6P is synthesized from uridine diphosphate-glucose and glucose-6-phosphate by the activity of T6P SYNTHASES (TPS) and converted to trehalose by T6P PHOSPHATASES (TPP), which is then hydrolysed into glucose by TREHALASES (TRE). Transgenic *Arabidopsis thaliana* plants with increased TPP activity in axillary buds have reduced T6P levels and delayed branch outgrowth, whilst plants with increased levels of T6P in the vasculature have enhanced branching[23]. Moreover, mutations in *Zea mays RAMOSA3* (*RA3*) and its paralog *ZmTPP4* that both encode TPP enzymes, lead to increased inflorescence branching[24,25]. Here, we found that all *PpTPS* genes were repressed after decapitation, whilst *PpTPP* and *PpTRE* genes were either repressed or induced, suggesting that T6P levels are dynamically regulated during the release of apical dominance. Besides, we found that *TPS* genes were IAA-induced and decapitation-repressed, and GO terms related to trehalose metabolism were associated with genes both induced by auxin and up-regulated after decapitation (Table S3), consistent with *TPP* and *TRE* expression profiles 2 and 6 h.a.d.. Thus, our data suggest that apically-produced auxin regulates the activity of T6P metabolic genes in the gametophore.

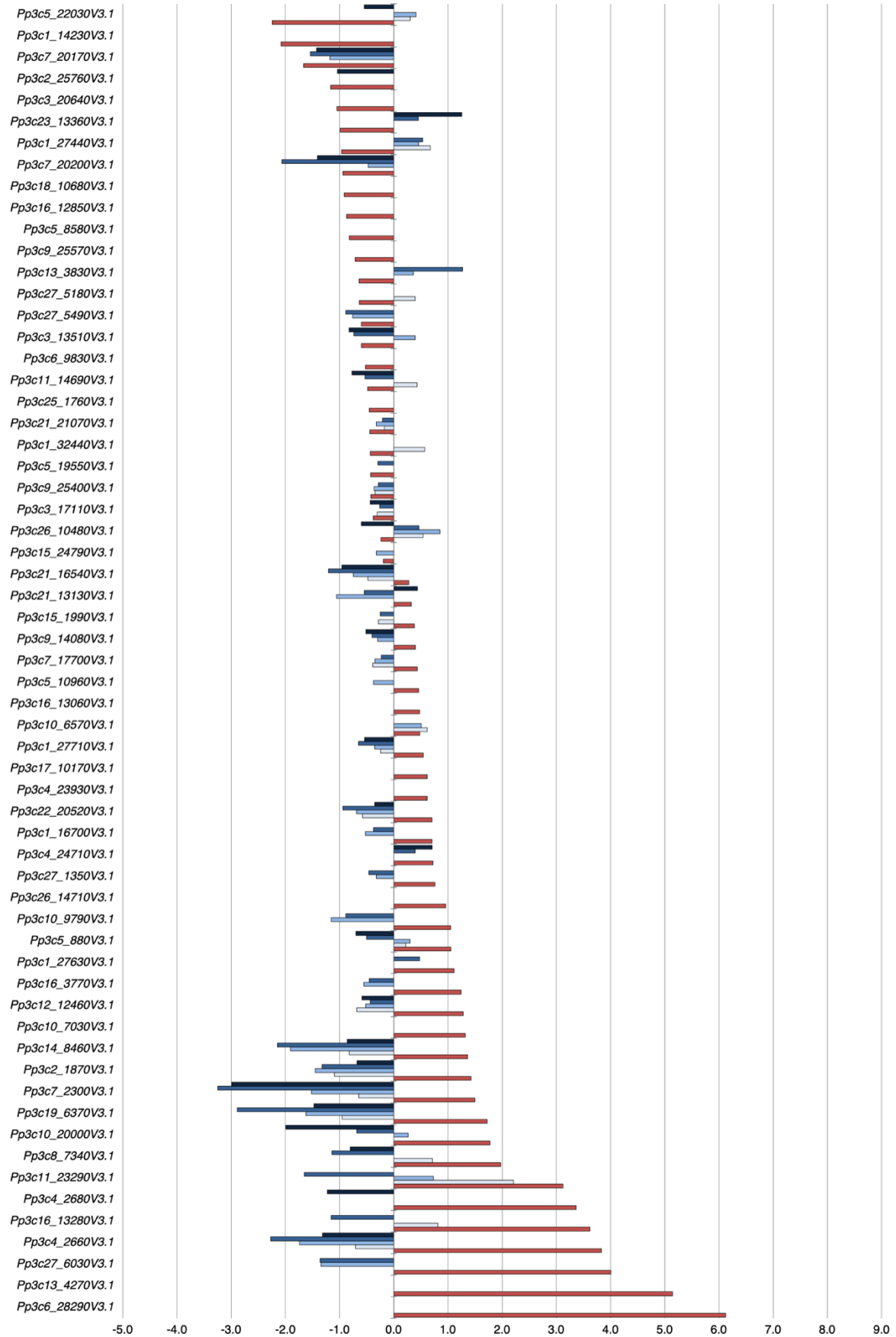
Pp3c5_22030V3.1
Pp3c1_14230V3.1
Pp3c7_20170V3.1
Pp3c2_25760V3.1
Pp3c3_20640V3.1
Pp3c23_13360V3.1
Pp3c1_27440V3.1
Pp3c7_20200V3.1
Pp3c18_10680V3.1
Pp3c16_12850V3.1
Pp3c5_8580V3.1
Pp3c9_25570V3.1
Pp3c13_3830V3.1
Pp3c27_5180V3.1
Pp3c27_5490V3.1
Pp3c3_13510V3.1
Pp3c6_9830V3.1
Pp3c11_14690V3.1
Pp3c25_1760V3.1
Pp3c21_21070V3.1
Pp3c1_32440V3.1
Pp3c5_19550V3.1
Pp3c9_25400V3.1
Pp3c3_17110V3.1
Pp3c26_10480V3.1
Pp3c15_24790V3.1
Pp3c21_16540V3.1
Pp3c21_13130V3.1
Pp3c15_1990V3.1
Pp3c9_14080V3.1
Pp3c7_17700V3.1
Pp3c5_10960V3.1
Pp3c16_13060V3.1
Pp3c10_6570V3.1
Pp3c1_27710V3.1
Pp3c17_10170V3.1
Pp3c4_23930V3.1
Pp3c22_20520V3.1
Pp3c1_16700V3.1
Pp3c4_24710V3.1
Pp3c27_1350V3.1
Pp3c26_14710V3.1
Pp3c10_9790V3.1
Pp3c5_880V3.1
Pp3c1_27630V3.1
Pp3c16_3770V3.1
Pp3c12_12460V3.1
Pp3c10_7030V3.1
Pp3c14_8460V3.1
Pp3c2_1870V3.1
Pp3c7_2300V3.1
Pp3c19_6370V3.1
Pp3c10_20000V3.1
Pp3c8_7340V3.1
Pp3c11_23290V3.1
Pp3c4_2680V3.1
Pp3c16_13280V3.1
Pp3c4_2660V3.1
Pp3c27_6030V3.1
Pp3c13_4270V3.1
Pp3c6_28290V3.1
-5.0
-4.0
-3.0
-2.0
-1.0
0.0
1.0
2.0
3.0
4.0
5.0
6.0
7.0
8.0
9.0

Figure S11.

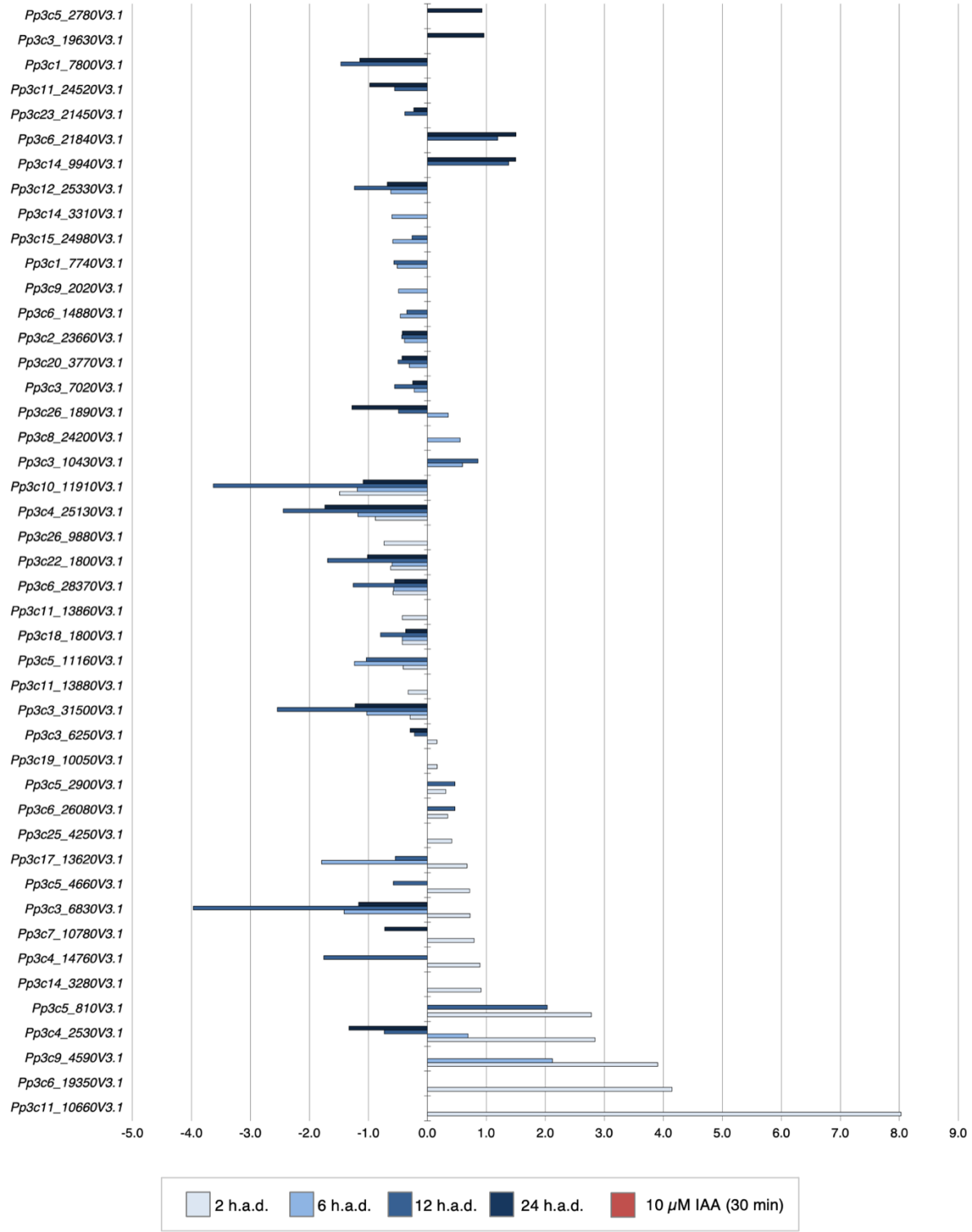

Figure S11 (continued). Expression of numerous *AP2/EREBP* genes is strongly affected by auxin and decapitation. Bar plots show *log2* fold-change in expression of genes associated with PFAM domain PF00847 (AP2-domain) in wild-type gametophores after auxin treatment (red bars) or decapitation (blue bars). GO analyses revealed a significant enrichment of the "DNA binding transcription factor activity" term in gene sets up- and down-regulated after decapitation (Table S2). Members of the *APETALA2/ETHYLENE-*

669 *RESPONSIVE ELEMENT BINDING PROTEIN* (*AP2/EREBP*) family represented about two
670 thirds of enriched DNA binding transcription factor coding genes and included putative
671 shared regulators of meristematic function, such as *STEMIN1* (*Pp3c1_27440v3.1*), known to
672 promote stem cell formation through local depletion of a repressive chromatin mark, and
673 *Pp3c26_9880v3.1*, the closest homologue to *Solanum lycopersicum LEAFLESS* and *A.*
674 *thaliana PUCHI* and *DORNRÖSCHEN-LIKE*, which are regulated by auxin and involved in
675 meristem identity and lateral organ initiation control[26–29].
676

Author contributions

MT and KL designed molecular constructs, generated transgenic lines and analyzed data ; SH, LST and VB produced RNA seq data and performed differential analyses ; NC performed statistical analyses ; YC designed the study, performed biological experiments with help from AM and GC, analyzed data and wrote the manuscript with input from all co-authors.

Acknowledgements

YC acknowledges Fabrice Besnard, Joe Cammarata, Pierre-Marc Delaux and Teva Vernoux for constructive discussions and suggestions on a draft version of this article, Stéphanie Hallet for technical support, Romain Azaïs for help with branching data analysis and the CNRS (ATIP-Avenir programme) for research funding. MT acknowledges the Swedish Research Council for funding (grant 2018-04068). The sequencing platform (POPS) benefited from the support of the LabEx Saclay Plant Sciences-SPS (ANR-10-LABX-0040-SPS).

References

1. Cline, M. (1991). Apical dominance. The Botanical Review *57*, 318–358.

2. Thimann, K., and Skoog, F. (1933). Studies on the growth hormone of plants: III. The inhibiting action of the growth substance on bud development. Proc Natl Acad Sci USA *19*, 714.

3. Skoog, F., and Thimann, K.V. (1934). Further Experiments on the Inhibition of the Development of Lateral Buds by Growth Hormone. Proc Natl Acad Sci U S A *20*, 480–485.

4. Balla, J., Medveďová, Z., Kalousek, P., Matiješčuková, N., Friml, J., Reinöhl, V., and Procházka, S. (2016). Auxin flow-mediated competition between axillary buds to restore apical dominance. Scientific Reports, 1–11.

5. Prusinkiewicz, P., Crawford, S., Smith, R.S., Ljung, K., Bennett, T., Ongaro, V., and Leyser, O. (2009). Control of bud activation by an auxin transport switch. Proc Natl Acad Sci USA *106*, 17431–17436.

6. Yadav, S., Kumar, H., and Yadav, R.K. (2020). Local auxin biosynthesis promotes shoot patterning and stem cell differentiation in Arabidopsis shoot apex. bioRxiv, 819342.

7. Galvan-Ampudia, C.S., Cerutti, G., Legrand, J., Brunoud, G., Martin-Arevalillo, R., Azais, R., Bayle, V., Moussu, S., Wenzl, C., Jaillais, Y., et al. (2020). Temporal integration of auxin information for the regulation of patterning. eLife *9*, e55832.

8. Cheng, Y., Dai, X., and Zhao, Y. (2006). Auxin biosynthesis by the YUCCA flavin monooxygenases controls the formation of floral organs and vascular tissues in Arabidopsis. Genes Dev. *20*, 1790–1799.

9. Wang, Q., Kohlen, W., Rossmann, S., Vernoux, T., and Theres, K. (2014). Auxin Depletion from the Leaf Axil Conditions Competence for Axillary Meristem Formation in Arabidopsis and Tomato. The Plant Cell *26*, 2068–2079.

10. Wang, Y., Wang, J., Shi, B., Yu, T., and Qi, J. (2014). The Stem Cell Niche in Leaf Axils Is Established by Auxin and Cytokinin in Arabidopsis. Plant Cell.

11. Coudert, Y., Bell, N.E., Edelin, C., and Harrison, C.J. (2017). Multiple innovations underpinned branching form diversification in mosses. New Phytol *22*, 810.

12. Coudert, Y., Palubicki, W., Ljung, K., Novak, O., Leyser, O., and Harrison, C.J. (2015). Three ancient hormonal cues co-ordinate shoot branching in a moss. eLife *4*, e06808.

13. Von Maltzahn, K. (1959). Interaction between Kinetin and Indoleacetic Acid in the Control of Bud Reactivation in Splachnum ampullaceum (L.) Hedw. Nature *183*, 60–61.

14. Lavy, M., Prigge, M.J., Tao, S., Shain, S., Kuo, A., Kirchsteiger, K., Estelle, M., and Hardtke, C.S. (2016). Constitutive auxin response in Physcomitrella reveals complex interactions between Aux/IAA and ARF proteins. eLife Sciences *5*, e13325.

15. Landberg, K., Šimura, J., Ljung, K., Sundberg, E., and Thelander, M. (2021). Studies of moss reproductive development indicate that auxin biosynthesis in apical stem cells may constitute an ancestral function for focal growth control. New Phytologist *229*, 845–860.

16. Thelander, M., Landberg, K., and Sundberg, E. (2018). Auxin-mediated developmental control in the moss Physcomitrella patens. J Exp Bot *69*, 277–290.

17. Ljung, K. (2013). Auxin metabolism and homeostasis during plant development. Development *140*, 943–950.

18. Eklund, D.M., Thelander, M., Landberg, K., Ståldal, V., Nilsson, A., Johansson, M., Valsecchi, I., Pederson, E.R.A., Kowalczyk, M., Ljung, K., et al. (2010). Homologues of the Arabidopsis thaliana SHI/STY/LRP1 genes control auxin biosynthesis and affect growth and development in the moss Physcomitrella patens. Development *137*, 1275–1284.

19. Proust, H., Hoffmann, B., Xie, X., Yoneyama, K., Schaefer, D.G., Yoneyama, K., Nogué, F., and Rameau, C. (2011). Strigolactones regulate protonema branching and act as a quorum sensing-like signal in the moss Physcomitrella patens. Development.

20. Decker, E.L., Alder, A., Hunn, S., Ferguson, J., Lehtonen, M.T., Scheler, B., Kerres, K.L., Wiedemann, G., Rizi, V.S., Nordzieke, S., et al. (2017). Strigolactone biosynthesis is evolutionarily conserved, regulated by phosphate starvation and contributes to resistance against phytopathogenic fungi in a moss, Physcomitrella patens. New Phytol *216*, 455–468.

21. Cline, M. (1997). Concepts and terminology of apical dominance. Am J Bot *84*, 1064.

753 22. Fichtner, F., Barbier, F.F., Feil, R., Watanabe, M., Annunziata, M.G., Chabikwa, T.G.,
754 Höfgen, R., Stitt, M., Beveridge, C.A., and Lunn, J.E. (2017). Trehalose 6-phosphate is
755 involved in triggering axillary bud outgrowth in garden pea (Pisum sativum L.). The Plant
756 Journal *92*, 611–623.

757 23. Fichtner, F., Barbier, F.F., Annunziata, M.G., Feil, R., Olas, J.J., Mueller-Roeber, B.,
758 Stitt, M., Beveridge, C.A., and Lunn, J.E. (2021). Regulation of shoot branching in
759 arabidopsis by trehalose 6-phosphate. New Phytol *229*, 2135–2151.

760 24. Satoh-Nagasawa, N., Nagasawa, N., Malcomber, S., Sakai, H., and Jackson, D.
761 (2006). A trehalose metabolic enzyme controls inflorescence architecture in maize.
762 Nature *441*, 227–230.

763 25. Claeys, H., Vi, S.L., Xu, X., Satoh-Nagasawa, N., Eveland, A.L., Goldshmidt, A., Feil,
764 R., Beggs, G.A., Sakai, H., Brennan, R.G., et al. (2019). Control of meristem determinacy
765 by trehalose 6-phosphate phosphatases is uncoupled from enzymatic activity. Nature
766 Plants, 1–9.

767 26. Toyokura, K., Goh, T., Shinohara, H., Shinoda, A., Kondo, Y., Okamoto, Y., Uehara,
768 T., Fujimoto, K., Okushima, Y., Ikeyama, Y., et al. (2019). Lateral Inhibition by a Peptide
769 Hormone-Receptor Cascade during Arabidopsis Lateral Root Founder Cell Formation.
770 Dev Cell *48*, 64-75.e5.

771 27. Chandler, J.W., and Werr, W. (2017). DORNRÖSCHEN, DORNRÖSCHEN-LIKE, and
772 PUCHI redundantly control floral meristem identity and organ initiation in Arabidopsis. J
773 Exp Bot *68*, 3457–3472.

774 28. Capua, Y., and Eshed, Y. (2017). Coordination of auxin-triggered leaf initiation by
775 tomato LEAFLESS. Proc Natl Acad Sci USA *114*, 3246–3251.

776 29. Ishikawa, M., Morishita, M., Higuchi, Y., Ichikawa, S., Ishikawa, T., Nishiyama, T.,
777 Kabeya, Y., Hiwatashi, Y., Kurata, T., Kubo, M., et al. (2019). Physcomitrella STEMIN
778 transcription factor induces stem cell formation with epigenetic reprogramming. Nat
779 Plants *5*, 681–690.

780 30. Romani, F. (2017). Origin of TAA Genes in Charophytes: New Insights into the
781 Controversy over the Origin of Auxin Biosynthesis. Front. Plant Sci. *8*, R899-3.

782 31. Delaux, P.-M., Hetherington, A.J., Coudert, Y., Delwiche, C., Dunand, C., Gould, S.,
783 Kenrick, P., Li, F.-W., Philippe, H., Rensing, S.A., et al. (2019). Reconstructing trait
784 evolution in plant evo-devo studies. Curr. Biol. *29*, R1110–R1118.

785 32. Eklund, D.M., Ishizaki, K., Flores-Sandoval, E., Kikuchi, S., Takebayashi, Y.,
786 Tsukamoto, S., Hirakawa, Y., Nonomura, M., Kato, H., Kouno, M., et al. (2015). Auxin
787 Produced by the Indole-3-Pyruvic Acid Pathway Regulates Development and Gemmae
788 Dormancy in the Liverwort Marchantia polymorpha. The Plant Cell Online *27*, 1650–1669.

789 33. Coudert, Y. (2017). The Evolution of Branching in Land Plants: Between
790 Conservation and Diversity. In Evolutionary Developmental Biology (Springer
791 International Publishing), pp. 1–17.

792 34. Solly, J.E., Cunniffe, N.J., and Harrison, C.J. (2017). Regional Growth Rate
793 Differences Specified by Apical Notch Activities Regulate Liverwort Thallus Shape.
794 Current Biology *27*, 16–26.

795 35. Puttick, M.N., Morris, J.L., Williams, T.A., COX, C.J., Edwards, D., kenrick, paul,
796 Pressel, S., Wellman, C.H., Schneider, H., Pisani, D., et al. (2018). The Interrelationships
797 of Land Plants and the Nature of the Ancestral Embryophyte. Current Biology, 1–16.

798 36. Morris, J.L., Puttick, M.N., Clark, J.W., Edwards, D., kenrick, paul, Pressel, S.,
799 Wellman, C.H., Yang, Z., Schneider, H., and Donoghue, P.C.J. (2018). The timescale of
800 early land plant evolution. Proceedings of the National Academy of Sciences *115*,
801 E2274–E2283.

802 37. Harris, B.J., Harrison, C.J., Hetherington, A.M., and Williams, T.A. (2020).
803 Phylogenomic Evidence for the Monophyly of Bryophytes and the Reductive Evolution of
804 Stomata. Current Biology *30*, 2001-2012.e2.

805 38. Edwards, D., Morris, J.L., Axe, L., Duckett, J.G., Pressel, S., and Kenrick, P. (2022).
806 Piecing together the eophytes – a new group of ancient plants containing cryptospores.
807 New Phytologist *233*, 1440–1455.

808 39. Harrison, C.J., and Morris, J.L. (2017). The origin and early evolution of vascular
809 plant shoots and leaves. Philosophical Transactions of the Royal Society of London B:
810 Biological Sciences *373*, 20160496–14.

811 40. Kenrick, P. (2018). Changing expressions: a hypothesis for the origin of the vascular
812 plant life cycle. Philos Trans R Soc Lond, B, Biol Sci *373*.

813 41. Shubin, N., Tabin, C., and Carroll, S. (1997). Fossils, genes and the evolution of
814 animal limbs. Nature *388*, 639–648.

815 42. Shubin, N., Tabin, C., and Carroll, S. (2009). Deep homology and the origins of
816 evolutionary novelty. Nature *457*, 818–823.

817 43. Hiss, M., Meyberg, R., Westermann, J., Haas, F.B., Schneider, L., Schallenberg-
818 Rüdinger, M., Ullrich, K.K., and Rensing, S.A. (2017). Sexual reproduction, sporophyte
819 development and molecular variation in the model moss Physcomitrella patens:
820 introducing the ecotype Reute. The Plant Journal *22*, 9.

821 44. Coudert, Y., Novák, O., and Harrison, C.J. (2019). A KNOX-Cytokinin Regulatory
822 Module Predates the Origin of Indeterminate Vascular Plants. Current Biology *29*, 2743-
823 2750.e5.

824 45. Thelander, M., Landberg, K., and Sundberg, E. (2019). Minimal auxin sensing levels
825 in vegetative moss stem cells revealed by a ratiometric reporter. New Phytologist *224*,
826 775–788.

827 46. Schaefer, D., Zryd, J.P., Knight, C.D., and Cove, D.J. (1991). Stable transformation
828 of the moss Physcomitrella patens. Mol Gen Genet *226*, 418–424.

829 47. Rensing, S.A., Lang, D., Zimmer, A.D., Terry, A., Salamov, A., Shapiro, H.,
830 Nishiyama, T., Perroud, P.-F., Lindquist, E.A., Kamisugi, Y., et al. (2008). The
831 Physcomitrella genome reveals evolutionary insights into the conquest of land by plants.
832 Science *319*, 64–69.

833 48. Gagnot, S., Tamby, J.-P., Martin-Magniette, M.-L., Bitton, F., Taconnat, L.,
834 Balzergue, S., Aubourg, S., Renou, J.-P., Lecharny, A., and Brunaud, V. (2008). CATdb: a

835 public access to Arabidopsis transcriptome data from the URGV-CATMA platform.
836 Nucleic Acids Research *36*, D986–D990.

837 49. Kopylova, E., Noé, L., and Touzet, H. (2012). SortMeRNA: fast and accurate filtering
838 of ribosomal RNAs in metatranscriptomic data. Bioinformatics *28*, 3211–3217.

839 50. Langmead, B., and Salzberg, S.L. (2012). Fast gapped-read alignment with Bowtie
840 2. Nat Methods *9*, 357–359.

841 51. Rigaill, G., Balzergue, S., Brunaud, V., Blondet, E., Rau, A., Rogier, O., Caius, J.,
842 Maugis-Rabusseau, C., Soubigou-Taconnat, L., Aubourg, S., et al. (2018). Synthetic data
843 sets for the identification of key ingredients for RNA-seq differential analysis. Briefings in
844 Bioinformatics *19*, 65–76.

845 52. McCarthy, D.J., Chen, Y., and Smyth, G.K. (2012). Differential expression analysis of
846 multifactor RNA-Seq experiments with respect to biological variation. Nucleic Acids
847 Research *40*, 4288–4297.

848 53. Heberle, H., Meirelles, G.V., da Silva, F.R., Telles, G.P., and Minghim, R. (2015).
849 InteractiVenn: a web-based tool for the analysis of sets through Venn diagrams. BMC
850 Bioinformatics *16*, 169.

851 54. Ge, S.X., Jung, D., and Yao, R. (2020). ShinyGO: a graphical gene-set enrichment
852 tool for animals and plants. Bioinformatics *36*, 2628–2629.

853 55. Edgar, R., Domrachev, M., and Lash, A.E. (2002). Gene Expression Omnibus: NCBI
854 gene expression and hybridization array data repository. Nucleic Acids Research *30*,
855 207–210.

856 56. Lang, D., Ullrich, K.K., Murat, F., Fuchs, J., Jenkins, J., Haas, F.B., Piednoel, M.,
857 Gundlach, H., Van Bel, M., Meyberg, R., et al. (2018). The Physcomitrella patens
858 chromosome-scale assembly reveals moss genome structure and evolution. The Plant
859 Journal *93*, 515–533.

860 57. Livak, K.J., and Schmittgen, T.D. (2001). Analysis of Relative Gene Expression Data
861 Using Real-Time Quantitative PCR and the 2−ΔΔCT Method. Methods *25*, 402–408.

862 58. Kleiber, C., and Zeileis, A. (2020). AER: Applied Econometrics with R.

863 59. Muff, S., Nilsen, E.B., O'Hara, R.B., and Nater, C.R. (2021). Rewriting results
864 sections in the language of evidence. Trends in Ecology & Evolution *0*.

865 60. Ortiz-Ramírez, C., Hernandez-Coronado, M., Thamm, A., Catarino, B., Wang, M.,
866 Dolan, L., Feijó, J.A., and Becker, J.D. (2016). A Transcriptome Atlas of Physcomitrella
867 patens Provides Insights into the Evolution and Development of Land Plants. Mol Plant
868 *9*, 205–220.

869